Deanship of Graduate Studies

Al-Quds University

Characterization of two variants in OSTM1 gene in osteopetrosis -affected Palestinian families.

Maram Ali Shawkat Eid

M.Sc. Thesis

Jerusalem-Palestine

1446/ 2025

Characterization of two variants in OSTM1 gene in osteopetrosis -affected Palestinian families.

Prepared by:

Maram Ali Shawkat Eid

B. Sc in Biotechnology and Genetic engineering /

Jordan University of Science and Technology/ Jordan

Supervisor: Dr. Zaidoun Salah

A thesis submitted in partial fulfillment of the requirements for the degree of Master of Medical Laboratory Science in the Diagnostic Microbiology and Immunology Track at the Faculty of Health Professions, AL-Quds University

1446/2025

Al-Quds University
Deanship of Graduate Studies
Biochemistry and Molecular Biology
Faculty of Medicine

Thesis Approval

Characterization of two variants in OSTM1 gene in osteopetrosis -affected Palestinian families.

Prepared By: Maram Ali Shawkat Eid
Registration No: 21920139

Supervisor: Dr. Zaidoun Salah

Master thesis submitted and accepted: 15/01/2025
The names and signatures of the examining committee members are as follows:

1- Head of Committee: Dr. Zaidoun Salah Signature:

2- Internal Examiner: Dr. Kifaya Suleiman Signature:

3- External Examiner: Prof. Hisham Darwish Signature:

Jerusalem-Palestine

1446 – 2025

Dedication

I humbly dedicate this work to my beloved parents, whose unwavering support has been my guiding light. To my cherished husband, Mohammad, your patience, and encouragement have been my rock. To my precious daughter, Eliaa, your innocent spirit is my constant inspiration. To my siblings, teachers, and friends, your belief in me has fuelled my determination. Lastly, this work is my modest offering to our beloved country.

Maram Ali Shawkat Eid

Declaration:

I certify that this thesis submitted for the degree of Master, is the result of my own research, except where otherwise acknowledged, and that this study (or any part of the same) has not been submitted for a higher degree to any other university or institution.

Signed: 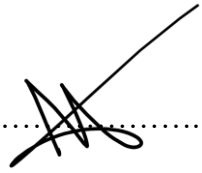 …….

Maram Ali Shawkat Eid

Date: 15/01/2025

Acknowledgment

First and foremost, I would like to express my gratitude to God for granting me the strength and guidance to complete this thesis.

I am grateful to my parents and my husband, Mohammad, who are my pillars of strength. I am beyond blessed to have them in my life.

I am deeply indebted to Augusta Victoria Hospital (AVH) for its generous funding, which was instrumental in the success of this research.

I also want to express my gratitude to the people who agreed to be part of our research. Their limitless help and patience with us were truly appreciated. I want to extend a special thanks to Basha’r, who helped us communicate with the families.

I am extremely thankful to my supervisor, Dr. Zaidoun Salah, and my department head, Dr. Musa Hindiyeh, for their unwavering support, invaluable guidance, and patience throughout this process. Their contributions have played a crucial role in shaping this thesis.

Abbreviations

OSTM1	Osteoclastogenesis-associated transmembrane protein 1
WES	Whole Exome Sequencing
BMPs	Bone morphogenetic proteins
WNT	Wingless-related integration site
BMD	Bone mineral density
M-CSF	Macrophage colony-stimulating factor
RANKL	Receptor activator of NF-κB ligand
c-Fms	Colony-stimulating Factor-1 Receptor
RANK	Receptor activator of NF-κB
CCL2	Chemoattractant (C-C) ligand-2
CAMs	Cell adhesion molecules
DC-STAMP	Dendritic cell-specific transmembrane protein
OC-STAMP	Osteoclast stimulatory transmembrane protein
Atp6v0d2	v-ATPase subunit d2
ITAM	Immunoreceptor tyrosine-based activation motif
DAP12	DNAX-activating protein 12
FcRγ	Fc receptor common γ subunit
TRAP	Tartrate-resistant acid phosphatase
CATK	Cathepsin K
Tfam	Mitochondrial transcription factor A
OPG	Osteoprotegerin
PTHrP	Parathyroid hormone (PTH)-related peptide
ADO	Autosomal dominant osteopetrosis (ADO)
IAO	'Intermediate' autosomal osteopetrosis (IAO)
MIOP	Malignant infantile osteopetrosis

KDa	Kilo-Dalton
ClC-7	Chloride channel 7
KIF5B	Kinesin family member 5B
OS	Mature retina's outer segments
RPE	Retinal pigmented epithelium
DNA	Deoxyribonucleic acid
PCR	Polymerase chain reaction
NCBI	National Center for Biotechnology Information
mRNA	Messenger ribonucleic acid
cDNA	Complementary DNA
dNTPs	Deoxynucleotide Triphosphates
DMSO	Dimethyl sulfoxide
TAE	Tris-Acetate-EDTA
EtBr	Ethidium Bromide
kp	Kilobase Pair
bp	Base Pair
ExoSAP	exonuclease I and shrimp alkaline phosphatase
EDTA	Ethylenediaminetetraacetic acid
RNA	Ribonucleic acid
RBC lysis	Red blood cell lysis
DPBS	Dulbecco’s phosphate-buffered saline
WT	Wild Type
SPIP	Splicing Prediction Pipeline
TGF-β	Transforming growth factor beta
EFNB2	Ephrin B2
EPHB4	Ephrin Receptor B4

NRP1	Neuropilin 1
SEMA3A	Semaphorin 3A
Igf-1	Insulin-like Growth Factor 1
WNT5A	Wnt Family Member 5A
S1P	Sphingosine 1-phosphate
CTHRC1	Collagen triple helix repeat containing 1
C3	Complement component 3

List of Figures

List of Tables

List of Appendices

Characterization of two variants in OSTM1 gene in osteopetrosis -affected Palestinian families.

Prepared by: Maram Ali Eid

Supervisor: Dr. Zaidoun Salah

Abstract

Background: Osteopetrosis is a rare genetic disorder characterized by increased bone density and brittle bones. Most cases result from mutations affecting lysosome-related organelle genes. One of the genes associated with osteopetrosis is the OSTM1 gene. Mutations in OSTM1 gene are linked to severe forms of the disease. Whole Exome Sequencing (WES) test was conducted on a group of affected Palestinian families, revealing two new variants c.365T>A (p.Val122Asp) and c.108C>T (p.Gly36Gly) in the OSTM1 gene. To our knowledge, these two variants have not been previously reported as pathogenic. Therefore, the study aims to determine their contribution to osteopetrosis.

Methods: In order to evaluate the pathogenicity of these two genetic variants, whole blood samples were collected from each family member of the inflicted families. DNA and RNA were extracted from each sample. Variant segregation was performed following Sanger sequencing on the obtained samples from the affected volunteers and their extended families' members. For the c.108 C>T (p.Gly36Gly) variant, which is hypothesized to create a donor splicing site, analysis was undertaken to look for splicing events that could result from the indicated variant. Primers flanking exons one and two were used to determine whether this variant results in abnormal splice variants of the OSTM1 gene.

Results: Segregation of the two variants was assessed by examining their inheritance in 36 participants. The results revealed that unaffected individuals possess both variants either in a heterozygous or wild-type genotype, while affected individuals are homozygous for both variants, indicating a recessive inheritance pattern. RNA analysis of the c.108 C>T (p.Gly36Gly) variant in the OSTM1 gene was also performed. The findings demonstrated that this variant does not affect splicing, contrary to claims made in a 2013 case report by Mahmoud et al., suggesting that the variant might create a donor splice site. This also goes against the predictions made by splicing prediction tools, indicating that the c.108 C>T (p.Gly36Gly) variant could potentially function as a splice site.

Conclusion: This study provided an opportunity to uncover the genetic variant responsible for the disease in the included families. Our results indicate that the variant c.365T>A (p.Val122Asp) segregates well between affected and unaffected family members, however, c.108C>T (p.Gly36Gly) variant does not affect splicing and thus seems to be a benign or neutral variant. This knowledge can help identify those at risk and provide preventative

interventions, improving patient counselling and raising awareness about the importance of premarital screening for the pathogenic variant of the OSTM1 gene.

Keywords: Osteopetrosis, OSTM1 gene, Segregation analysis, RNA analysis, c.365T>A, p.Val122Asp, c.108C>T, p.Gly36Gly, point mutation, missense mutation.

Table of Contents

1. Chapter One

1.1 Introduction

Bone tissue maintains a delicate balance through a dynamic process known as bone remodelling or homeostasis. This process involves continuous cycles of bone formation and resorption, maintained by specialized cells in the bone tissue called osteoclasts and osteoblasts (Jung-Min et al., 2020; Udagawa et al., 2021). These cells work together through direct contact and interactions between EFNB2-EPHB4, FAS-FASL, and NRP1-SEMA3A to maintain harmony within bone structure, (**Figure 1.1**) (Jung-Min et al., 2020).

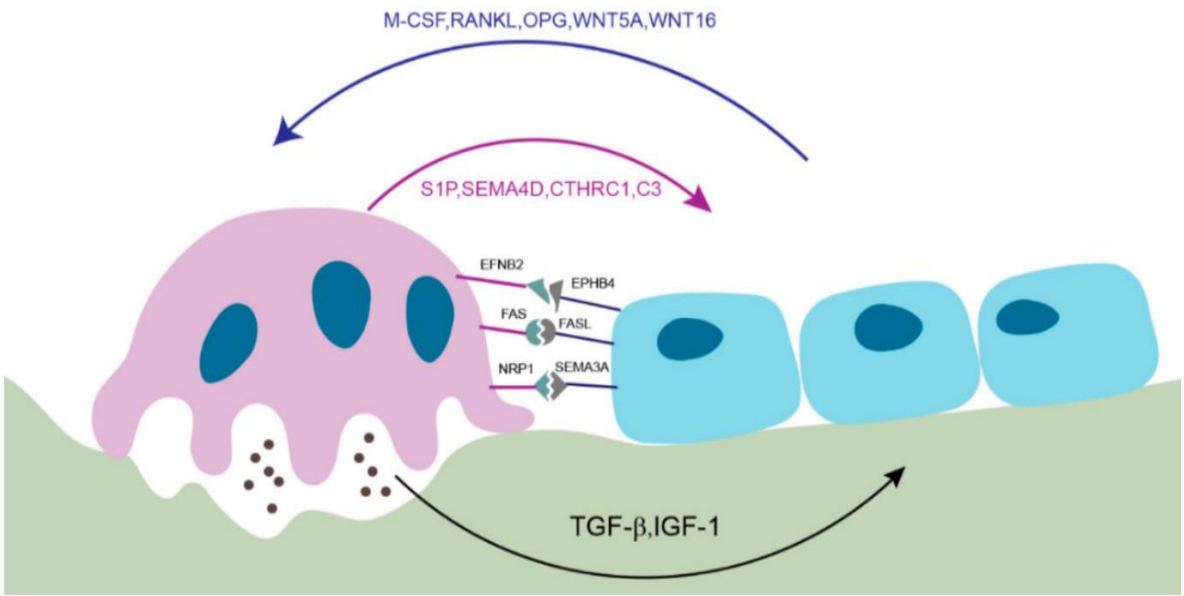

Figure 1.1: Overview of Osteoclast-Osteoblast interactions. These cells interact directly through various pathways, including EFNB2-EPHB4, FAS-FASL, and NRP1-SEMA3A, to regulate their activities. Osteoclast-mediated bone resorption releases TGF-β and IGF-1, promoting osteoblast-mediated bone formation. Osteoblasts secrete M-CSF, RANKL, and WNT5A to promote osteoclast formation and development, while osteoclasts secrete S1P, CTHRC1, and C3 to promote osteoblast differentiation. (Jung-Min et al., 2020).

1.1.1 Osteoblast:

Osteoblast cells develop from multipotent marrow stromal stem cells, also known as mesenchymal precursors, through a complex process involving many genes, transcription factors, and miRNAs that promote the differentiation of osteoblasts toward the osteogenic lineage. Primarily, these molecular factors belong to bone morphogenetic proteins (BMPs) and wingless-related integration site (WNT) pathways. However, other pathways are also involved, including the nuclear factor κB pathway, typically associated with osteoclasts, and the NAD+-dependent deacetylase sirtuin-1 pathway, responsible for forming new bone (Ponzetti, , Rucci, & 2021; Titorencu et al., 2014).

Osteoclasts initiate bone formation by releasing S1P, CTHRC1, and C3, stimulating osteoblast differentiation (Jung-Min et al., 2020). Once activated, osteoblasts start producing the organic component of bones called osteoid, primarily composed of collagen. A crucial step in bone formation is the process of mineralization, where minerals such as calcium and phosphate crystallize around the collagen scaffold to form hydroxyapatite, the major inorganic constituent of bone. This process is essential for the strength and rigidity of bones (Ponzetti et al., 2021; Titorencu et al., 2014). Bone mineral density (BMD) can be used to estimate the strength of bones and assess the risk of fractures (Al-Bari et al., 2020). As osteoblasts build new bone tissue, they become embedded within bone structure and transform into osteocyte tissues. Another type of mature osteoblasts are bone-lining cells, which are inactive osteoblasts that provide complete coverage of bone surface and acts as a barrier for ions (Titorencu et al., 2014). Consequently, osteoblasts release M-CSF, RANKL, and WNT5A, which promote differentiation of osteoclasts. Osteoclasts, in turn, secrete SEMA4D, which inhibits the development of new bone by interfering with osteoblast formation, initiating the process of bone resorption (Jung-Min et al., 2020).

1.1.2 Osteoclasts:

Osteoclasts, characterized by their multinucleated structure which contains numerous mitochondria in their cytoplasm (Vacher et al., 2020), play a crucial role in bone remodelling and regulating calcium balance within the body. Originating from monocytes in the bone marrow, osteoclasts release vital minerals such as calcium phosphate and biologically active molecules, including growth factors, from the bone matrix (Al-Bari, , Al Mamun, & 2020; Boyle et al., 2003; Udagawa et al., 2021).

The process of osteoclast formation, known as osteoclastogenesis, is complex. It involves the fusion of mononuclear precursors into multinucleated cells known as polykaryons (Boyle et al., 2003). A central aspect of this process is the role of osteoblasts, which secrete the macrophage colony-stimulating factor (M-CSF), and the receptor activator of NF-κB ligand (RANKL). These factors release specific signals that bind to osteoclast receptors, initiating the process of osteoclastogenesis (**Figure 1.2**). Analysis of Colony-stimulating Factor-1 Receptor (c-Fms), a receptor for M-CSF, and receptor activator of NF-κB (RANK), a receptor for RANKL, revealed the significant role of immunoglobulin-like receptors in osteoclast differentiation (Al-Bari et al., 2020; Boyle et al., 2003). These immunoglobulin-like receptors play a pivotal role in the

signalling cascades that govern osteoclastogenesis, a process essential for bone resorption and remodelling. The interaction of RANKL with its receptor RANK, along with the presence of Osteoprotegerin (OPG) in this regulatory system, is crucial for determining the balance between osteoclast formation and inhibition. Specifically, RANKL binds to RANK on the surface of osteoclast precursors, triggering a series of intracellular signalling pathways that promote their differentiation into mature multinucleated osteoclasts. (Boyle et al., 2003; Jung-Min et al., 2020)

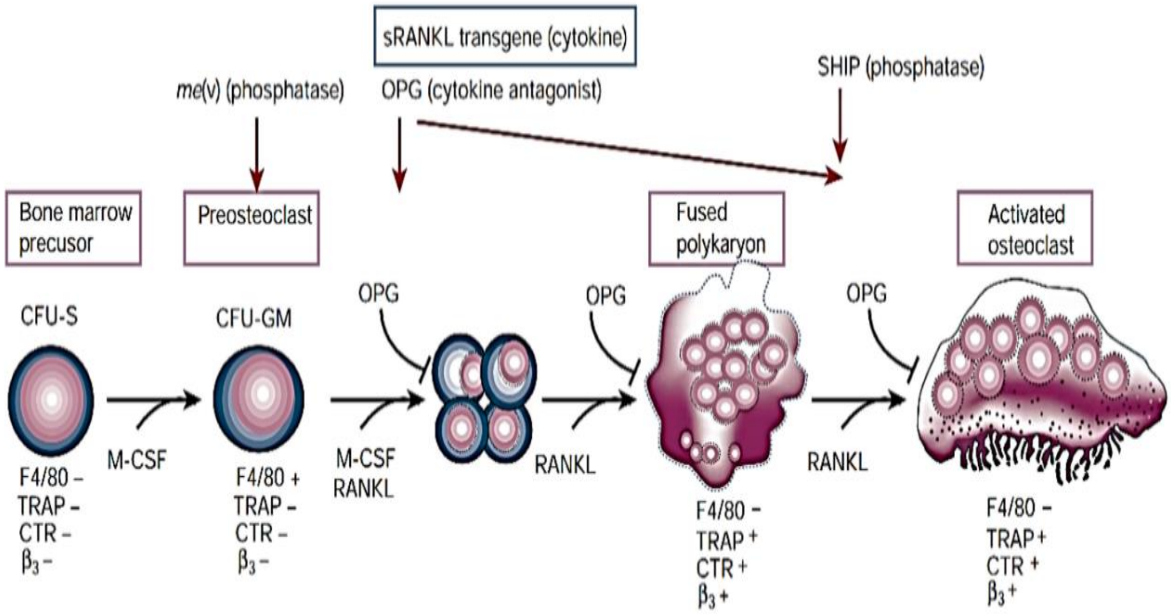

Figure 1.2: Osteoclast development. The image illustrates the process of hematopoietic precursor cells developing into mature osteoclasts, known as osteoclastogenesis. It shows the crucial roles of two key factors: Macrophage Colony-Stimulating Factor (M-CSF) and Receptor Activator of Nuclear Factor κ B Ligand (RANKL), essential for osteoclast formation. The diagram also discusses the influence of specific single-gene mutations that can disrupt normal osteoclast development and lead to various bone-related disorders. Furthermore, it explains the regulatory role of Osteoprotegerin (OPG), which inhibits osteoclast formation and activity by binding to RANKL, thereby neutralizing its function. This interaction is vital for maintaining bone homeostasis and preventing excessive bone resorption (Boyle et al., 2003).

The formation of multinucleated osteoclasts enhanced by RANKL requires the presence of the chemoattractant (C-C) ligand-2 (CCL2) and its receptor CCR2 (Takegahara et al., 2024). In addition, cell adhesion molecules (CAMs) icluding integrins and cadherins are necessary for committed osteoclasts to adhere to each other, establish close membrane contact, and organize their cytoskeleton. CAMs also play a role in coordinating RANKL-induced osteoclast differentiation as signal transduction molecules. Extensive rearrangements of the cytoskeleton occur during this phase. Committed osteoclasts eventually undergo cell-cell fusion, a process that involves several molecules, including dendritic cell-specific transmembrane protein (DC-STAMP), osteoclast stimulatory transmembrane protein (OC-STAMP), and v-ATPase subunit

d2 (Atp6v0d2). The expression of these fusion-related molecules is regulated by NFATc1 and c-Fos, which are downstream of RANKL-RANK signalling (Takegahara et al., 2024).

In addition, calcium signalling plays a role in osteoclast differentiation. Although RANK cannot directly activate calcium signalling, a study on a molecule called an immunoreceptor tyrosine-based activation motif (ITAM) that induces a calcium signal in immune system cells identified as DNAX-activating protein 12 (DAP12) and Fc receptor common γ subunit (FcRγ). It was reported that osteoclast differentiation was impaired in double-deficient mice, resulting in severe osteopetrosis. This finding underscores the essential nature of signals mediated by immunoglobulin-like receptors associated with DAP12 and FcRγ, which works as costimulatory signals for osteoclast differentiation (Al-Bari et al., 2020).

Upon maturation, circulating osteoclasts adhere to the surface of the bone matrix. This adhesion is a crucial initial step in a series of transformations that enable them to effectively perform their physiological role. During this phase, known as cytodifferentiation, these precursor cells undergo significant morphological and functional changes, transforming into mature osteoclasts. The mature osteoclasts develop a highly specialized structure that is vital for their interaction with the bone matrix. This structure is characterized by the formation of numerous delicate and intricate microvilli, which protrude from the cell membrane. (Mulari et al., 2003; Sobacchi et al., 2013; Vacher et al., 2020).

This structure involves an extensively folded plasma membrane region, creating a circumferential zone between the ruffled border surface and the bone matrix called the Howship's Lacuna. Within this space, osteoclasts release various organic acids, including citric acid and lactic acid, which are responsible for degrading the mineral component of bone (Mulari et al., 2003; Sobacchi et al., 2013; Vacher et al., 2020). Acidifying this compartment by secretion of protons leads to activating Tartrate-resistant acid phosphatase (TRAP) and Cathepsin K (CATK), the two main enzymes responsible for degrading bone mineral and collagen matrices. These acids and enzymes work together to break down the bone, allowing for the release of minerals and the remodelling of the bone structure (**Figure 1.3**) (Boyle et al., 2003).

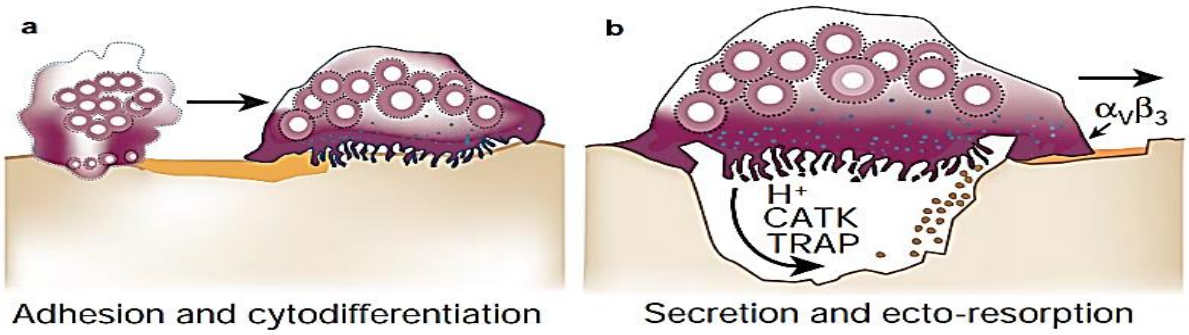

Figure 1.3: Osteoclast activity in bone remodelling. The figure illustrates mature osteoclasts adhering to the bone matrix, forming Howship's lacuna, and secreting degrading enzymes such as TRAP and CATK. These enzymes break down bone mineral and collagen matrices, allowing for mineral release and bone remodelling (Boyle et al., 2003).

The RANKL/RANK/OPG pathway negatively regulate the activity of mature osteoclasts through osteoprotegerin (OPG). OPG binds to and neutralizes RANKL, preventing it from binding to the RANK receptor on osteoclast precursors (Udagawa et al., 2021). This process helps maintain the delicate balance of bone resorption and formation within the skeletal system. Additionally, various hormones and factors such as TNF-a, IL-1b, vitamin D3, and parathyroid hormone (PTH)-related peptide (PTHrP) regulate bone resorption and calcium balance locally by triggering the expression of RANKL within bone cells.

T cells can also serve as a crucial source of RANKL in the bone (**Figure 1.4**) (Boyle et al., 2003). Other hormones and factors, like estrogens, decrease bone resorption and increase density by reducing RANKL activation and, subsequently, decrease the number of activated osteoclasts in the bone. Therefore, RANKL-deficient individuals may resist bone resorption induced by certain factors (Boyle et al., 2003; C.-H. Cheng et al., 2022).

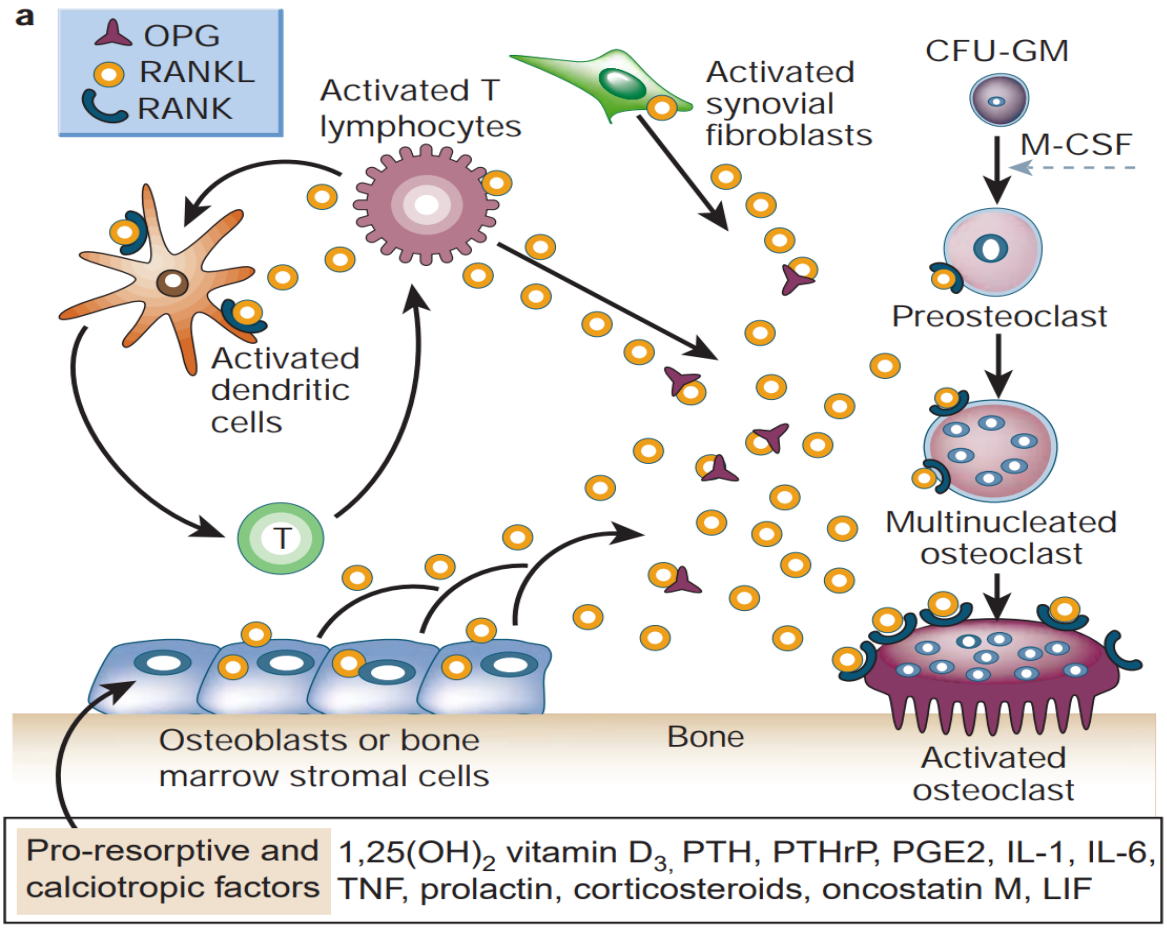

Figure 1.4: Hormonal regulation of bone homeostasis. This diagram shows how various hormones and factors, such as TNF-a, IL-1b, vitamin D3, and parathyroid hormone (PTH)-related peptide (PTHrP), produced in distant organs, regulate bone resorption and calcium balance locally by stimulating the expression of RANKL within bone cells. T cells also play a critical role as a source of RANKL in the bone. (Boyle et al., 2003).

Furthermore, the osteoclast plays a pivotal role in bone formation. It stimulates the release of several factors and enzymes, including transforming growth factor beta (TGF-β), from the bone matrix which acts directly on osteoclasts, promoting the secretion of Wnt1. Wnt1 then stimulates osteoblasts, which is an essential step in bone formation. In addition, osteoclast secretes exosomes that contain RANK, which migrate to osteoblasts. These RANK receptors bind to RANKL in osteoblasts, triggering a reverse signal that activates the PI3K–Akt pathway, thereby increasing osteoblast activity, as illustrated in (**Figure 1.5**) (Udagawa et al., 2021).

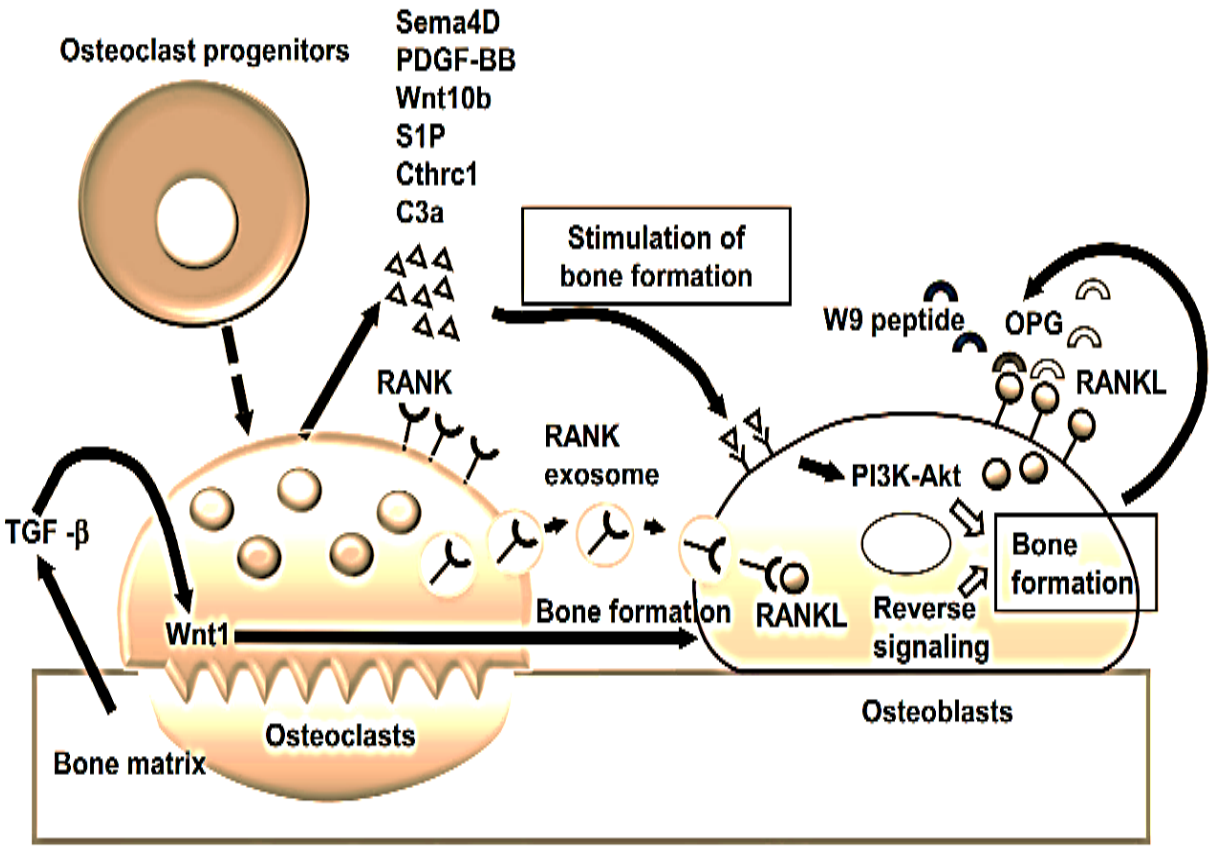

Figure 1.5: Osteoclast-dependent osteoblast activation. This illustration depicts the process of reverse signalling that activates osteoblasts due to osteoclast activity. The osteoclast triggers the release of factors and enzymes, such as TGF-β, from the bone matrix. TGF-β then promotes the secretion of Wnt1, which stimulates osteoblasts, essential for bone formation. Additionally, the osteoclast releases exosomes containing RANK, which activate the PI3K–Akt pathway, increasing osteoblast activity (Udagawa et al., 2021).

It is important to note that mutations in the mitochondrial transcription factors, especially the mitochondrial transcription factor A (Tfam), can also impair osteoclast function. Osteoclasts rely on significant amounts of ATP produced by the mitochondria for optimal function (Takegahara et al., 2024). This is why osteoclasts contain numerous mitochondria in their cytosol (Vacher et al., 2020).

The balance between bone-forming osteoblasts and bone-resorbing osteoclasts is crucial for bone remodelling. These cells, found in both the bone lining and within the bone itself, communicate through direct contact and secretory proteins, regulating their behaviour and differentiation. Factors like M-CSF, RANKL/OPG, Wnt1, and TGF-β play an important role in this communication. Understanding this process is important to comprehend the intricate process of bone remodelling. Disruption to this balance can lead to complications in bone structure and normal bone turnover and growth. Like osteopetrosis (Jung-Min et al., 2020).

1.1.3 Osteopetrosis:

Osteopetrosis is a rare group of genetic disorders that affect the growth and remodeling of bones. It causes an increase in bone density due to impaired osteoclast function, resulting in brittle and fragile bones that are more susceptible to fractures (Alotaibi, , Dighe, & 2021). The disease can cause various symptoms, such as osteosclerosis, pathologic fractures, pancytopenia, cranial neuropathies, skull foramina occlusion and hepatosplenomegaly in severe cases. Its name comes from "osteo," meaning bone, and "petrosis," meaning stone, due to increased bone density (Spinnato et al., 2022). The disease was first identified in 1904 by a German radiologist, Dr. Albers-Schonberg (Spinnato et al., 2022). Most osteopetrosis defects result from mutations that impair lysosome-related organelles' trafficking and/or fusion to the ruffled border, leading to a loss of function in the acidification process (Sobacchi et al., 2013; Vacher et al., 2020).

1.1.4 Diagnosis of osteopetrosis:

Radiographs, including X-rays, CT scans, and MRI, are essential for diagnosing and assessing the severity of osteopetrosis (Spinnato et al., 2022). These imaging techniques reveal widespread bone hardening throughout the skeleton, increased cortical thickness, and decreased medullary canal diameter. However, genetic testing is necessary to identify specific mutations associated with osteopetrosis and to distinguish between different subtypes, each requiring unique treatment approaches with varying prognoses and risks of recurrence (Wu et al., 2017). Genetic testing is crucial for accurate diagnosis. In cases where typical radiographic signs are absent, blood tests can aid in diagnosis (Wu et al., 2017). Elevated blood concentrations of creatine kinase BB isoenzyme and tartrate-resistant acid phosphatase (TRAP) can be helpful in these situations (Spinnato et al., 2022).

1.1.5 Classification and Pattern of inheritance:

Osteopetrosis is categorized into different types based on inheritance models and severity. It encompasses a wide range of genetic mutations, leading to diverse clinical symptoms, age of onset, and prognosis, ranging from mild to severe (Spinnato et al., 2022; Wu et al., 2017). Autosomal dominant osteopetrosis (ADO) is the most common form of osteopetrosis, with an incidence of approximately 1 in 20,000 (Chen et al., 2016; Sobacchi et al., 2013; Wu et al., 2017). It may not show symptoms and is often diagnosed by chance. Common symptoms include bone pain, increased frequency of fractures, and cranial nerve complications due to bony overgrowth. ADO has two distinct phenotypic types (Bollerslev, , Andersen, & 1988;

Sobacchi et al., 2013). Type I is characterized by massive skull sclerosis and cranial vault thickening with patients are often asymptomatic with no increased fracture risk (Spinnato et al., 2022). Type II is characterized by thickening of the pelvic end bones and may lead to various symptoms including anemia, pathologic fractures, bone pain, cranial nerve compression, or early arthritis in adulthood (Chen et al., 2016; Spinnato et al., 2022). The most common mutation in ADO type II involves mutations in the CLCN7 gene, leading to impaired osteoclasts (Chen et al., 2016). 'Intermediate' autosomal osteopetrosis (IAO) can be inherited in two different patterns, autosomal recessive or autosomal dominant. It is primarily caused by mutation in the CAH2 gene, responsible for producing carbonic anhydrase II protein (Shah et al., 2004; Spinnato et al., 2022). Symptoms typically appear during childhood and may include increased risk of bone fractures and anemia. Patients with this condition usually do not have life-threatening bone marrow abnormalities (Spinnato et al., 2022). However, some affected individuals may experience calcifications in brain, intellectual disability, and a type of kidney disease called renal tubular acidosis (Shah et al., 2004). This form of osteopetrosis is less severe than the malignant form, since affected individuals usually reach adulthood (Spinnato et al., 2022).

Infantile or "malignant" form of osteopetrosis is an autosomal recessive condition. It is a rare condition diagnosed in infancy, occurring in about 1 in 250,000 live births. It can be fatal within the first decade if untreated (Penna et al., 2021). The condition can have a range of complications, including an increased susceptibility to infections, dental issues such as cavities and facial bone infections, particularly post-dental surgery, and bone damage (Penna et al., 2021; Spinnato et al., 2022). The limited bone marrow space often leads to elevated number of hematopoietic stem and progenitor cells in the blood, further complicating the condition (Spinnato et al., 2022). Neurological issues can also arise (Alotaibi et al., 2023). This form of the disease also encompasses the X-linked variant of osteopetrosis, an extremely rare form with only a handful of unrelated patients reported in the literature (Palagano et al., 2018).

Autosomal recessive disorder, the most severe form of the disease, is mainly attributed to alterations in specific genes such as TCIRG1, OSTM1, CLCN7, RANK, and RANKL (Palagano et al., 2018; Spinnato et al., 2022). These genes can either affect the function of osteoclasts, leading to elevated defective osteoclasts, or affect the differentiation of osteoclasts, leading to a decrease in osteoclast count (Pillai et al., 2022). The rarest and most lethal form of malignant infantile osteopetrosis (MIOP) is often caused by mutations in the OSTM1 gene, which can lead to early mortality in infancy if left untreated. Hence, a better understanding of OSTM1-associated MIOP can aid in improved symptom management and early referral for palliative care (Alotaibi et al., 2021; Alotaibi et al., 2023).

1.1.6 OSTM1 gene:

The osteoclastogenesis-associated transmembrane protein 1 (OSTM1) gene is located on chromosome 6 (6q21) and comprises six exons and five introns (Ramírez et al., 2004). It encodes a 334 amino acid protein and is about 40 kb long (https://www.ncbi.nlm.nih.gov/nuccore/163965386). The mature OSTM1 protein undergoes post-translation processing and is heavily N-glycosylated with an approximate mass of 60 kDa

(Lange et al., 2006; Vacher et al., 2020). It is a luminal protein with only 30 cytosolic amino acids at the C-terminus and is highly conserved from flies to humans. OSTM1 protein is located in the cytosolic cellular compartment and is absent from the nuclear fraction, suggesting it is most likely a cytosolic protein (Chalhoub et al., 2003; Lange et al., 2006; Pata et al., 2021). According to Vacher J. and his coworkers (2020), the OSTM1 can interact with several cytosolic proteins and is involved in a multifunctional protein platform (Vacher et al., 2020).

Despite initial assumptions that OSTM1 protein was a type of E3 ubiquitin ligase, current studies refute this hypothesis (Vacher, 2022). Pathogenic variants in OSTM1 have been linked to autosomal recessive osteopetrosis, which can cause a severe form of the disease in infancy and often leads to death within the first few years of life (Alotaibi et al., 2021; Ramírez et al., 2004). In addition, mutations in the OSTM1 gene can trigger the development of lysosomal storage disease (Lange et al., 2006).

1.1.7 OSTM1 gene and its Role in Osteopetrosis:

OSTM1 is a type I transmembrane protein with a signal peptide, that is essential for interacting with the Chloride channel CLC-7 within osteoclasts' lysosomes (Zhang et al., 2020). This interaction results in the formation of an electrogenic Cl^-/H^+ antiporter, as illustrated in (**Figure 1.6**) (Lange et al., 2006).

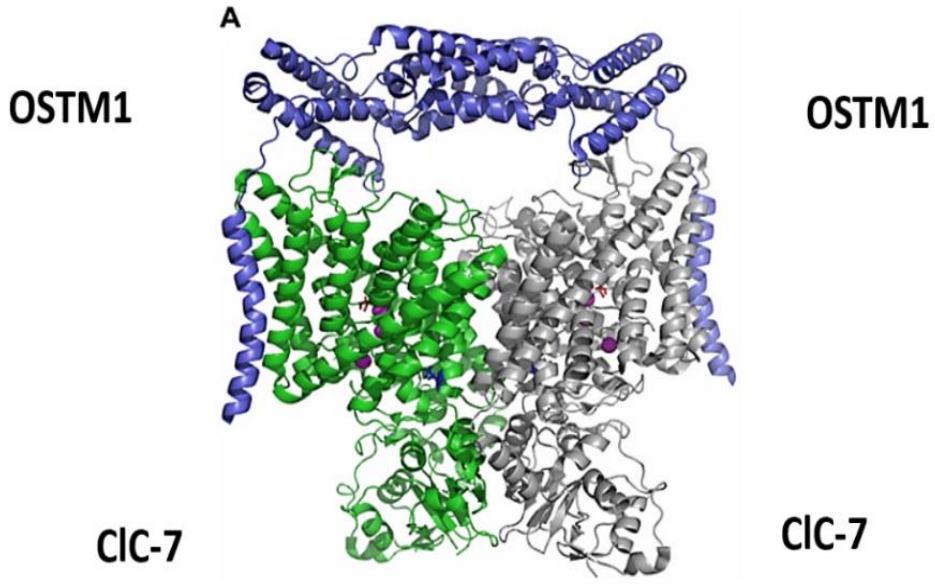

Figure 1.6: The structure of the ClC-7/OSTM1 complex. The ClC-7/OSTM1 complex, a vital protein assembly involved in cellular ion transport. In this representation, the OSTM1 subunits are distinctly highlighted in blue, while the ClC-7 subunits are depicted in a combination of green and gray colors. This color coding aids in differentiating the two types of subunits and emphasizes their unique roles within the complex. (Pusch, , Zifarelli, & 2021).

OSTM1 is a key protein that plays an essential role in maintaining the stability of CLC-7, a chloride channel important for various cellular processes. By binding to CLC-7, OSTM1 prevents its degradation within the lysosome, ensuring that CLC-7 remains functional and available for cellular activities (Sobacchi et al., 2013). The mechanism by which OSTM1 interacts with CLC-7 involves the formation of a dimeric structure. This dimer is heavily glycosylated, which refers to the presence of sugar molecules attached to it, enhancing its stability and functionality. Additionally, the dimer contains disulfide bonds, which contribute to the structural integrity of the complex (Schrecker, Korobenko, & Hite, 2020).

The transport of the OSTM1-CLC-7 complex to the osteoclast ruffled border is a critical step in bone resorption. The ruffled border is a specialized membrane structure that increases the surface area of osteoclasts, enhancing their ability to absorb bone tissue. This transport process is essential for the localization of CLC-7 and plays a significant role in the overall resorptive function of osteoclasts (Lange et al., 2006). Thus, the proper formation of the ruffled border is closely linked to osteoclast activity, highlighting the importance of OSTM1-mediated transport in bone remodeling (Vacher et al., 2020).

According to Vacher et al. (2020), the impact of OSTM1 mutations is not limited to destabilizing CLC-7 on the osteoclast ruffled membrane; it also affects the acidification of the osteoclast resorption lacuna, a crucial process for the release of lysosomal enzymes . This disruption leads to impaired trafficking of secretory lysosomes and prevents the formation of the ruffled border, ultimately resulting in the development of osteopetrosis. Interestingly, a mutation in the ClC-7 gene leads to a milder form of osteopetrosis compared to OSTM1 mutations, suggesting that OSTM1 may have additional, yet-to-be-discovered functions (Vacher et al., 2020).

OSTM1 is transported to the lysosome's chloride/proton exchanger CLC-7 with the assistance of Kinesin family member 5B (KIF5B). KIF5B is a motor protein that plays a vital role in the movement of cell components (Pandruvada et al., 2016). It interacts with OSTM1 through its heavy chain and OSTM1 C-terminus protein. Together, KIF5B and OSTM1 facilitate the transport of cargos within the cell from the endoplasmic reticulum to endosomes/lysosomes. Depletion of KIF5B results in the clustering of OSTM1 and lysosomes near the center of the cell, emphasizing the importance of their interaction in cell component movement. Similarly, the loss of OSTM1 leads to a different distribution of lysosomes within bone cells, highlighting OSTM1's direct role in facilitating cell component movement in partnership with KIF5B (**Figure 1.7**) (Pandruvada et al., 2016; Vacher et al., 2020).

In a study conducted by Pandruvada and colleagues in 2016, researchers examined the role of OSTM1 gene in relation to brain and hair pigmentation (Pandruvada et al., 2016). These findings are important as they confirm previous suspicions and enhance our understanding of mental retardation in affected individuals (Vacher, 2022). This suggests that the causes of mental retardation in osteopetrosis patients extend beyond the physical pressure exerted by

dense bone on cranial nerves and blood vessels. They also involve the complex functions of various genes, as explored by (Vacher et al., 2020) and (Alotaibi et al., 2023).

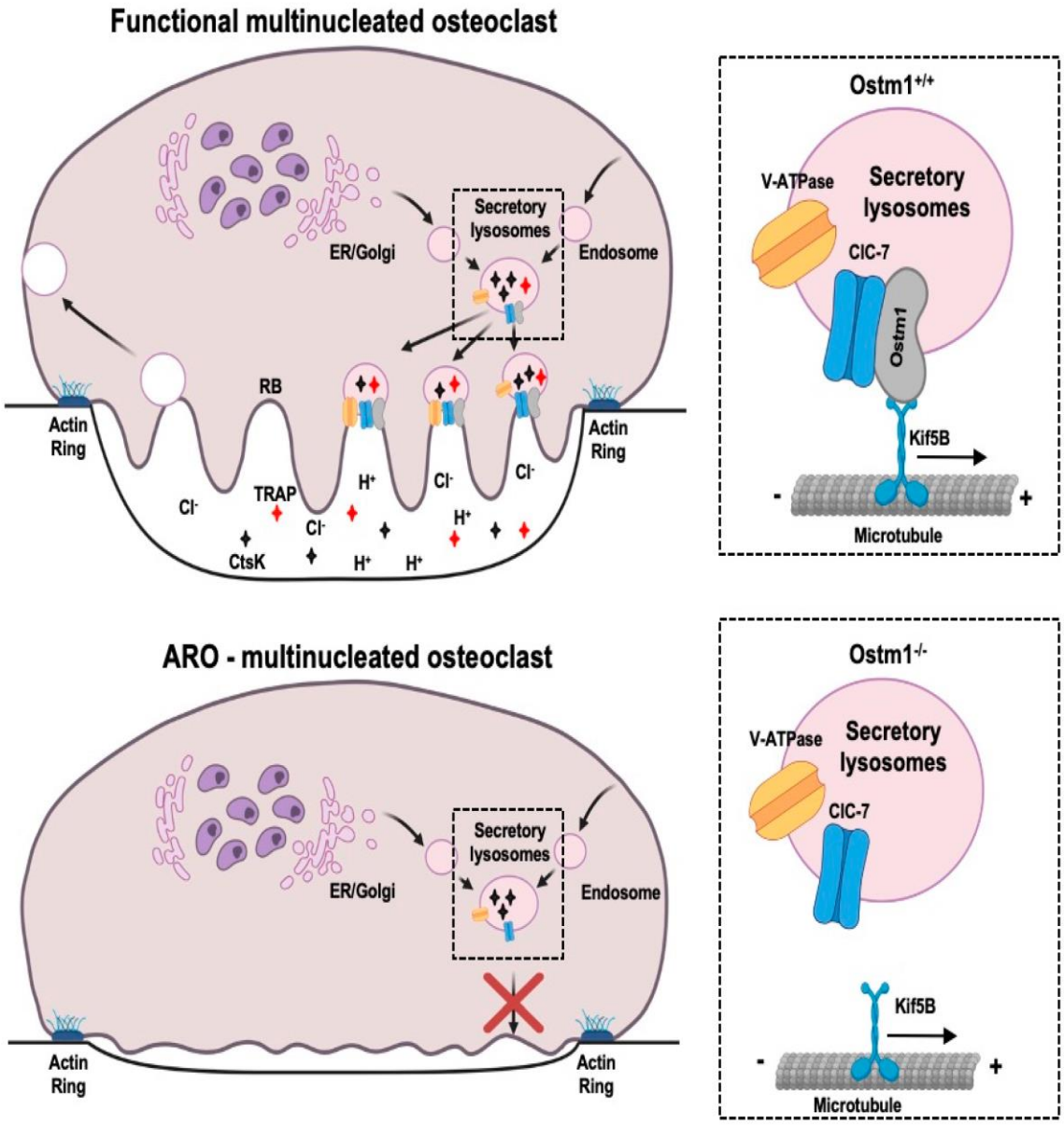

Figure 1.7: Consequences of OSTM1 malfunction on bone resorption. The image demonstrates how dysfunction of the OSTM1 protein disrupts the acidification of the resorption lacuna and the trafficking of secretory lysosomes, impairing ruffled border formation. The OSTM1 and CLC-7 complex is crucial for transporting CLC-7 to the osteoclast's ruffled border, essential for its resorption function. Additionally, OSTM1 is transported to the lysosome's chloride/proton exchanger CLC-7 with the help of KIF5B, a motor protein facilitating cell component movement. Depletion of KIF5B leads to the clustering of OSTM1 and lysosomes near the center of the cell, emphasizing their interaction in cell component movement. Similarly, the loss of OSTM1 leads to a different distribution of lysosomes within bone cells, highlighting OSTM1's role in facilitating cell component movement in partnership with KIF5B (Vacher et al., 2020).

1.1.8 Gene Expression:

The OSTM1 protein is widely expressed in a variety of embryonic hematopoietic, skeletal, and brain tissues. Notably, even after birth, OSTM1 maintains its presence in several critical postnatal tissues, including the gastrointestinal tract, kidneys, and skin (Vacher et al., 2020). In addition to the aforementioned tissues, OSTM1 expression has been documented in a diverse array of other anatomical structures, such as the nervous system, bone marrow, kidney, spleen, thymus, and osteoclasts. Additionally, it can be found in the outer segments (OS) and retinal pigmented epithelium (RPE) of the fully mature retina (Pandruvada et al., 2016; Pata et al., 2021). It has also been demonstrated that OSTM1 expression is significantly increased in the brain, spinal cord, and kidney, and to a lesser extent in the spleen, bone marrow, thymus, eye, testis, and primary osteoblasts, as shown in (**Figure 1.8**).

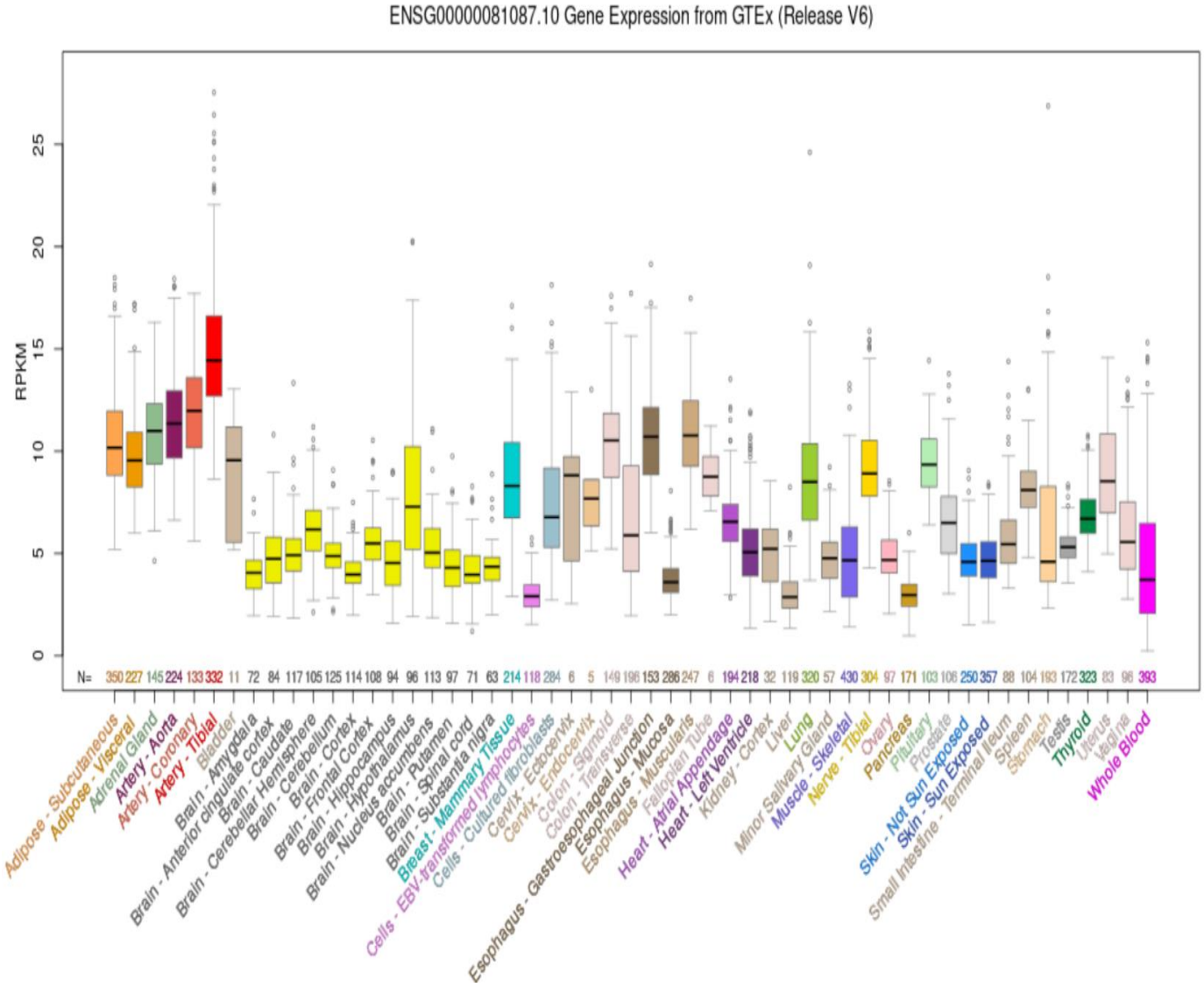

Figure 1.8: RNA-seq OSTM1 Gene Expression Data from GTEx. Provided by UCSC Genome Browser.

Studies in mice and humans have shown that OSTM1 deficiency is associated not only with bone health issues and severe osteopetrosis but also with neurological problems (Vacher, 2022). As a result, it is crucial to understand the specific cells where OSTM1 is expressed, especially within the nervous system (Pata et al., 2021). This highlights the pressing need to further explore the detailed implications of OSTM1 expression in the in the various parts of the nervous system, as depicted in (**Figure 1.9**).

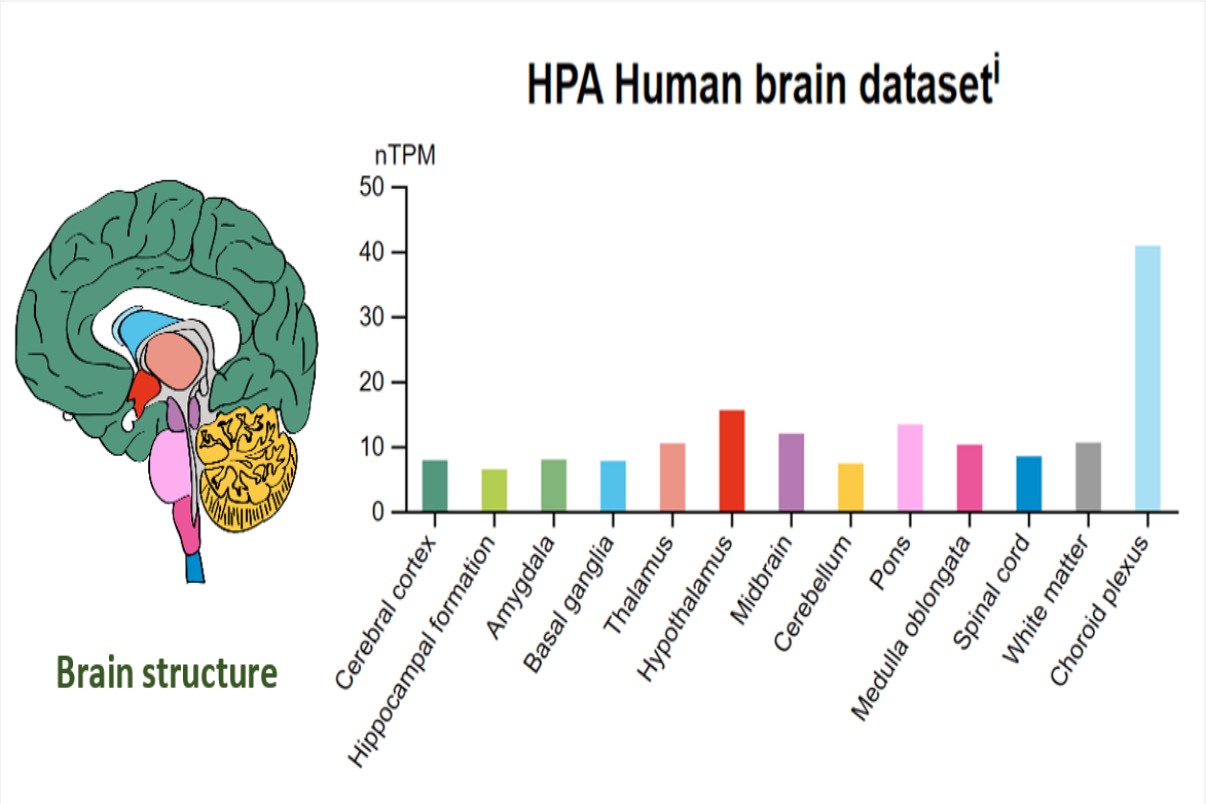

Figure 1.9: OSTM1 expression in the brain. OSTM1 Gene Expression Data in the brain from GTEx. Provided by GTEx.

According to a study by Pata M. et al (2021), immunohistochemistry analysis revealed the expression of OSTM1 protein in neuronal populations within the central and peripheral nervous systems . Strong signals were detected in specific types of neurons in the granular cell layer of the hippocampus, in layer V of the cortex, and in Purkinje cells of the cerebellum. In the lumbar spinal cord, OSTM1 expression seems to be restricted to motor neurons in the ventral horn, confirming that OSTM1 protein is cytosolic (Pata et al., 2021).

Furthermore, Patients with a defective OSTM1 protein often exhibit additional symptoms, including upper respiratory issues, hepatosplenomegaly (enlargement of the liver and spleen), difficulty feeding, and pancytopenia (Alotaibi et al., 2023; Ramírez et al., 2004; Souraty et al., 2007; Spinnato et al., 2022). These symptoms have been observed in multiple patients, and numerous studies have confirmed the significant role of OSTM1 gene in these tissues (Alotaibi et al., 2023; Vacher, 2022).

1.1.9 Mutations in OSTM1 Gene Associated with Osteopetrosis:

In 2003, Chalhoub and colleagues found that a mutation in the human OSTM1 gene causes severe recessive osteopetrosis. They examined the gene sequence in 19 patients with this condition and identified a specific mutation (IVS5+5G-A) in a patient of Italian origin, which was absent in 100 control subjects (Chalhoub et al., 2003). In 2004, Ramirez and colleagues reported a case involving a 3-month-old girl diagnosed with severe osteopetrosis. Genetic testing identified 2-base pair deletion (c.415_416delAG) in the OSTM1 gene. This deletion leads to a frameshift mutation, resulting in early stop codon and termination of the protein chain (Ramírez et al., 2004). Pangrazio et al. (2006) found the same deletion in unrelated Kuwaiti patients and a nonsense mutation c.36T>A (P.Cys12X) in a Lebanese boy (Pangrazio et al., 2006). In 2007, Mégarbané A. and colleagues conducted a study on six families from Middle Eastern countries, all of whom had children who met the clinical and radiological criteria for osteopetrosis. Molecular analysis revealed a common homozygous G>C mutation in two patients, at position +5 of the donor splice site in intron 5 of the OSTM1 gene (Souraty et al., 2007). In 2013, Mahmoud A. et al. discovered two mutations in the OSTM1 gene in a 9-month-old child from middle eastern origin with osteopetrosis, craniosynostosis and Chiari malformation type I with missense mutation (c.365T>A) and a (c.108C>T) transition resulting in a synonymous mutation (G36G). The unaffected first-cousin parents were heterozygous for both mutations (Mahmoud et al., 2013).

1.2 Problem statement and Study significance

Due to consanguineous marriages, autosomal recessive osteopetrosis is prevalent in our Palestinian communities, which has significant implications for public health. Therefore, studying mutations leading to this disease is essential for public health and the community (Hengel et al., 2020; Palagano et al., 2018). Our study focused on three Palestinian families to identify a potential causative mutation for osteopetrosis by analyzing results from a previously conducted whole-exome sequencing (WES) test on three affected patients (**Appendix 7.5**). The initial findings were intriguing. One patient had two homozygous variants, p.Val122Asp, and p.Gly36Gly, in the OSTM1 gene, both of which were of uncertain significance. The other two patients had only one variant, p.Val122Asp, which was also present in the first patient.

Preliminary analysis of exon 1 of the OSTM1 gene in two affected families indicated that both parents were heterozygous for the c.108C>T and c.365T>A variants. The presence of these variants in the OSTM1 gene, along with the high degree of relatedness among the families, suggests that they may contribute to the development of the disease.

Additionally, we noted a case report by Mahmoud et al. (2013) that documented a 9-month-old baby with both the c.365T>A and c.108C>T variants. However, that study could not establish the pathogenic nature of either variant, resulting in inconclusive findings due to a lack of evidence(Mahmoud et al., 2013). Identifying the variants in our patients was crucial for determining the potential impact of these OSTM1 variants on the development of the disorder. This important step will improve our understanding of the disease and facilitate the development of more effective interventions and preventive measures to halt the transmission of this life-

threatening disease across the new generations of inflicted families with potential for broader application.

1.3 Aims and objectives

The primary objective of this investigation is to identify the genetic variant(s) responsible for osteopetrosis in the participating families and to raise awareness about the importance of premarital screening for pathogenic variants in the OSTM1 gene. This screening can help identify at-risk individuals, enabling the provision of preventive strategies thorough effective counselling and assist families in avoiding the birth of new patients with osteopetrosis.

2. Chapter Two

2.1 Materials and methods

2.1.1 Patients:

The study involved thirty-six family members from three Palestinian families, all of whom have a relative affected by osteopetrosis. The probands' grandparents, parents, siblings, and some of their aunts and uncles were included in our study. These families hail from the town of Idnah, west of Hebron, in the West Bank, and have willingly participated in the study. The Ethics Committee of Augusta Victoria Hospital in Jerusalem rigorously reviewed and approved the study see, (**Appendix 7.4**). Each participant received an informed consent form, which they agreed to and signed. Parental consent was also obtained for participants under the age of eighteen (**Appendix 7.3**).

Figures 10, 11, and 12 display the family pedigrees. All pedigrees were created using the QuickPed website.

The first family, (**Figure 2.1**), has two affected members. Both parents in one of those subfamilies have been confirmed to be heterozygous for both variants (III-6) site see, (**Appendix 7.6**), indicating a potential autosomal recessive inheritance pattern. In the other subfamily (III-7), the parents of the affected member with ARO are suspected to be heterozygous, at least for one of the two variants, suggesting a similar inheritance pattern.

The second family, (**Figure 2.2**), is particularly interesting due to its relationship to the first family. In this family, two members have osteopetrosis, but only one has been genetically tested and was found to have two homozygous variants, p.Val122Asp, and p.Gly36Gly, in the OSTM1 gene. The other member has been diagnosed with the condition only based on clinical observation. Importantly, family (II-9) mutually connects with the first family.

The last family, (**Figure 2.3**), has one affected member. The family reported that both parents (III-4) of the affected member and one of their siblings are carriers (heterozygous) for the (c.365 T>A) variant. It's worth mentioning that these three families are related to each other through their grandmother.

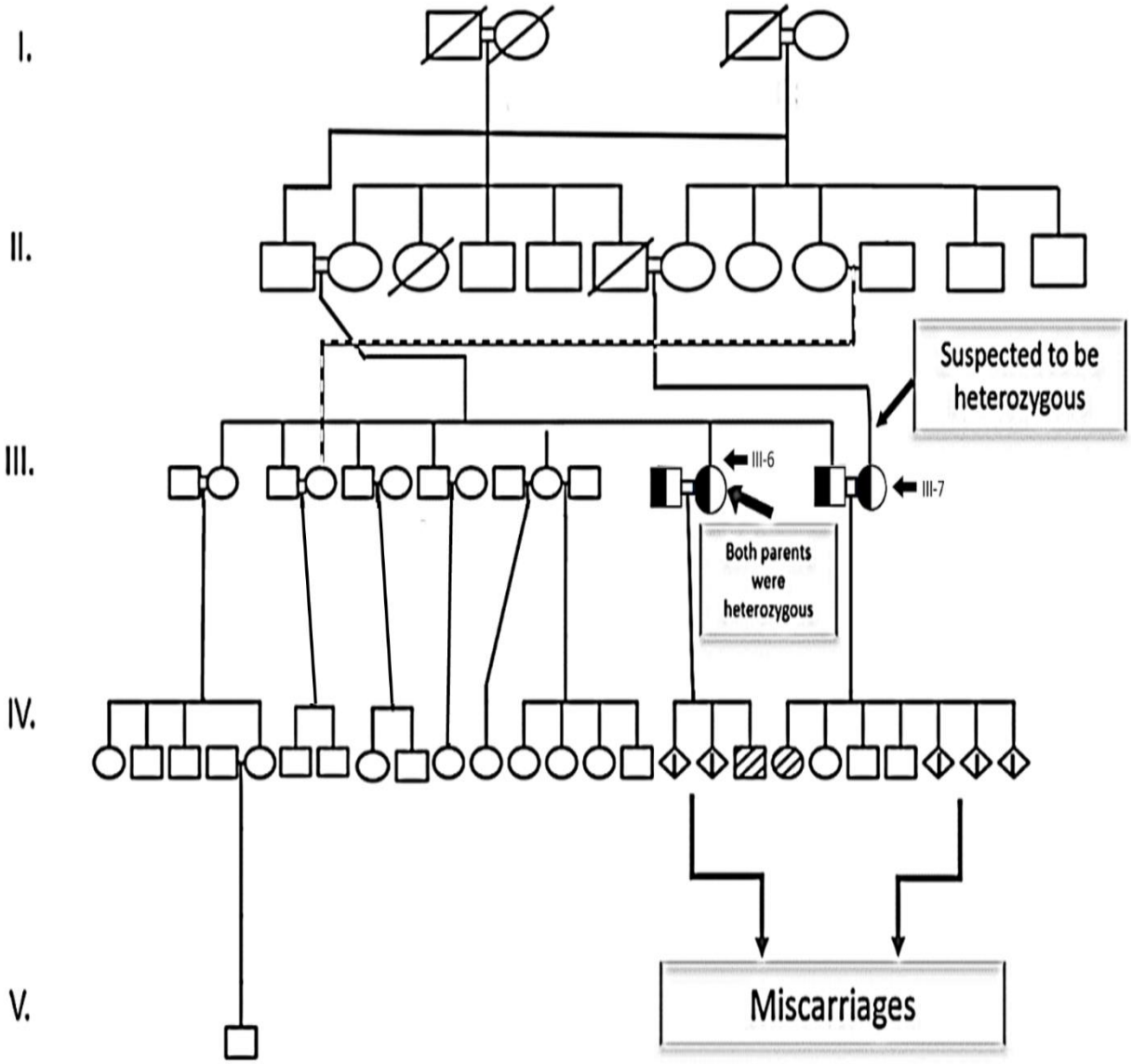

Figure 2.1: The pedigree of family 1: shows six participating families with two affected members**.** In one of those families, the parents of the affected member have been confirmed to be heterozygous for both variants. It is suspected that the parents of the other affected member are also heterozygous. In the pedigree, squares represent males and circles represent females. The diagonal line through a symbol indicates that the individual is deceased. Half-shaded symbols signify carriers, while multiple diagonal lines represent affected individuals.

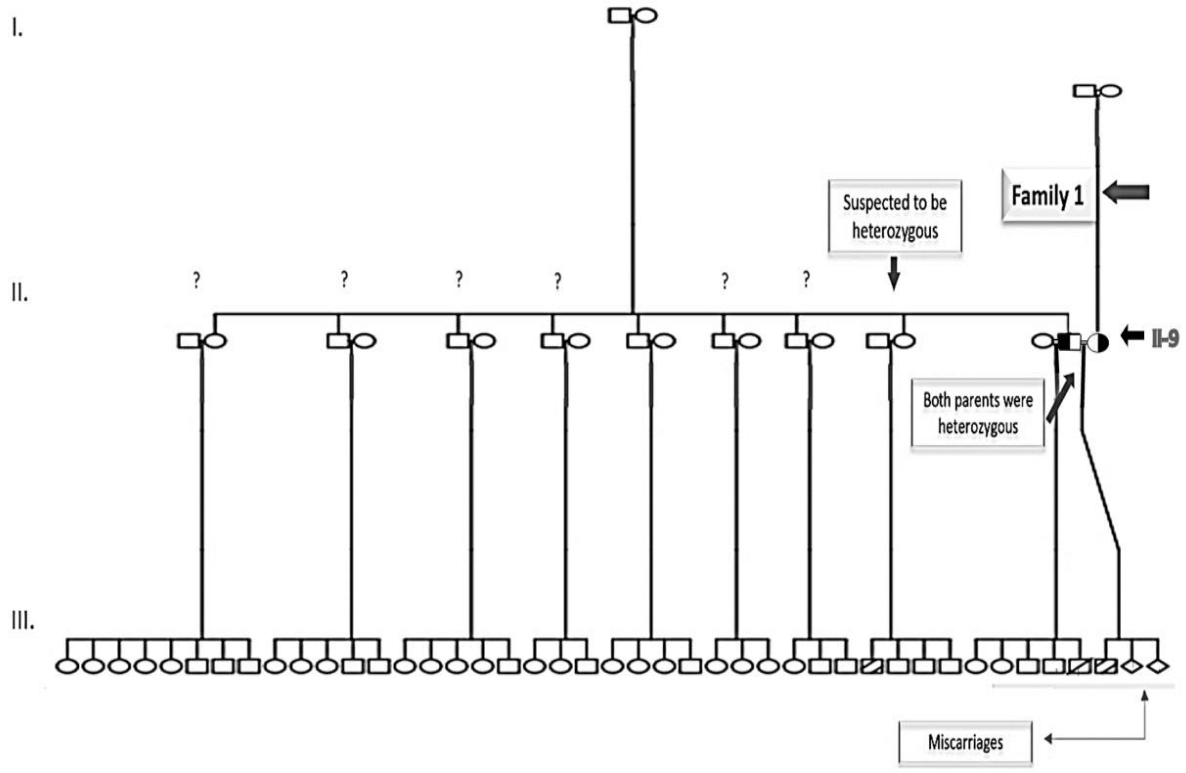

Figure 2.2: The pedigree of family 2: shows two participating families, each with one affected member. Family (II-9) shares a connection with the first family and is shown in the previous pedigree. . In the pedigree, squares represent males and circles represent females. Half-shaded symbols signify carriers, while multiple diagonal lines represent affected individuals.

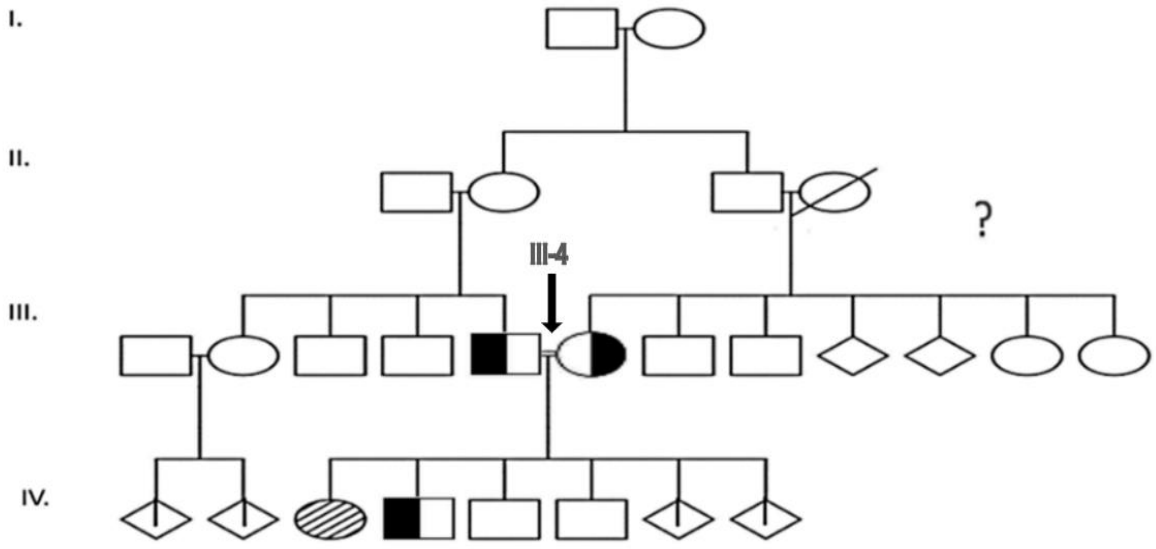

Figure 2.3: **The pedigree of family 3:** This diagram shows two families with one affected member each. Squares denote males, circles denote females, and diagonal lines indicate deceased individuals. Half-shaded symbols represent carriers, while multiple diagonal lines indicate affected individuals.

2.1.2 DNA extraction:

DNA was extracted from EDTA peripheral blood samples. The extraction process was carried out using the fully automated nucleic acid extraction instrument magLEAD® 12Gc from PSS. This instrument employs magtration technology to separate magnetic beads. First, samples were swiftly transferred to a well containing the lysis buffer which includes proteinase K and lysis solution. Magnetic beads were then added to the lysed cells in order to bind nucleic acids and discard the lysis and buffer. The magnetic beads were then washed twice using alcohol-containing washing buffers. Finally, the nucleic acid was eluted and transferred to a fresh tube. The concentration of the extracted DNA samples was measured using nanodrop 2000c Spectrophotometer from Thermo-Scientific.

2.1.3 Primer Design:

In this study, sequence data was obtained from the National Center for Biotechnology Information (NCBI) website to design primers for both the mRNA region (https://www.ncbi.nlm.nih.gov/nuccore/NM_014028.4) and the genomic region (https://www.ncbi.nlm.nih.gov/nuccore/163965386) of the OSTM1 gene. Primers were designed using the Primer3web version 4.1.0 software (http://primer3.ut.ee). For Sanger sequencing, one forward and reverse primers were designed to cover the location of the two variants in exon 1 (**refer to Appendix 7.1, Table 7.1**). For testing the effect of Gly36Gly variant on OSTM1 RNA splicing, two primers were designed. One reverse primer is located in exon one, and the other covers part of exon two (**refer to Appendix 7.1, Table 7.2**). UCSC In-Silico PCR tool (https://genome.ucsc.edu/cgi-bin/hgPcr) was used to verify the primers specificity, and the primer's annealing temperatures were calculated using the Promega Tm Calculator (https://worldwide.promega.com/resources), which considers the GoTaq buffer composition as well as the primers' GC content.

2.1.4 In silico analysis:

We utilized several software tools, including Polyphen, PhD-SNP, Clinvar, AlphaMissence server, Alphafold-3 and Mutation Taster, to assess the pathogenicity of the two variants. Additionally, we used alignment tools such as Clustal Omega and Cobalt to evaluate the conservation of valine in the c.Val122Asp variant. Nucleotide BLAST alignment tool (https://blast.ncbi.nlm.nih.gov/Blast.cgi) to compare the obtained sequences with the reference sequence (NG_007262.1) and two different tools were utilized SPIP and RNA splicer to predict the effect of the genetic variant (c.108 C>T) on mRNA splicing.

2.1.5 Polymerase chain reaction (PCR):

The GoTaq® G2 Green Master Mix (Promega, Cat# M7822), a premixed ready-to-use solution, was used. The components of the PCR reaction mixture are shown in (**Table 2.1**).

Table 2.1: Amounts of reagents used in PCR reaction preparation.

Contents / Final concentration	**1x Reaction (ul)**
GoTaq Mix (1X)	*12.5 ul*
Forward + Reverse primer	*1.5 ul*
DNA Template (80-100 ng)	*Up to 5 ul*
D.W	*6 ul*
Total Volume Mix	*25 ul*

The volume of each component was adjusted based on the number of reactions needed. A no-template control (NTC) was added to each mix, a critical step that eliminates the possibility of nucleic acid contamination and ensures the reliability of our results. Additionally, 1 ul of 1% dimethyl sulfoxide (DMSO) was introduced into the cDNA reaction mix. DMSO disrupts base pairing and effectively reduces the melting temperature (Tm), thereby enhancing the PCR process.

Gradient PCRs were initially employed to determine the optimal annealing temperature for the PCR runs. Afterward, the PCR cycling conditions were established as follows: an initial incubation step at 95°C for 3 minutes, followed by 40 cycles of denaturation at 95°C for 30 seconds, annealing at 65°C for 30 seconds of the DNA template, and annealing at 60°C for 30 seconds of the cDNA template, followed by an extension at 72°C for 1 minute. It concluded with a final extension step at 72°C for 5 minutes and then the mixture was held at 12°C. The process was conducted using the C1000 Touch™ PCR thermal cycler from BIO-RAD.

2.1.6 Gel electrophoresis:

To ensure successful amplification of the PCR product, a 1.5% agarose gel was prepared by mixing 150 mL of 1X TAE buffer and 2.25 g of the agarose powder obtained from Hylabs (Cat# KI 8100-500). The agarose-TAE mixture was heated for 2 minutes until completely dissolved and then cooled for about 3 minutes. After cooling, Ethidium Bromide (EtBr) (Hylabs, Cat# BP451) was added to achieve a final concentration of approximately 0.2 to 0.5 µg/mL. The agarose was then poured into a casting tray with two well combs in place and left to solidify at room temperature for 20-25 minutes.

Once solidified, the agarose gel was placed into the chamber filled with 1X TAE buffer. A 100 bp DNA ladder RTU (Hylabs, BIO-HELIX, and Cat # DM001-R500) was loaded into the gel chamber well, followed by 5 µL of each PCR product to the additional wells. The DNA visualization was conducted under UV light using the Molecular Imager Gel DOCTM XR+ Imaging System from BIO-RAD.

2.1.7 Sanger sequencing:

Following the PCR reaction, the PCR products underwent purification using ExoSAP-IT™ PCR Product Cleanup Reagent (Applied Biosystems, Cat# 78201.1ML). This reagent consists of exonuclease I (Exo) and shrimp alkaline phosphatase (SAP) to eliminate excess primers and unincorporated nucleotides. 2ul of ExoSAP solution was combined with 5 ul of each PCR product. Then, the reaction was carried out in a C1000 Touch™ PCR thermal cycler from BIO-RAD at 37°C for 30 minutes, followed by an incubation step at 80°C for 15 minutes to deactivate the enzymes. The purified PCR products were then stored at -20°C until use to maintain their stability and quality.

Sanger sequencing was then performed on the purified products using the BigDye Terminator Ready Reaction mix to sequence the PCR product. Each sequencing reaction consisted of 1 ul of Big Dye Terminator v1.1 Cycle Sequencing (Applied Biosystems, Cat# 4336774), 3.5 ul of 5X buffer (Applied Biosystems, Cat# 4336697), and 2 ul of 5uM primer (Hylabs), either forward or reverse, combined with 11.5 ul of molecular-grade water (Sartorius, Cat# 01-869-1A) and 2 ul of the clean PCR product. The reagents, each with its specific quantity, required for each sequencing reaction are listed in (**Table 2.2**).

After preparing the reaction mixes, the plate (Applied Biosystems, Cat# 4306737) was spun down briefly. Afterwards, the sequencing reactions took place in Veriti™ 96-Well Fast Thermal Cycler from Applied Biosystems according to the following program: an initial incubation step at 96°C for 1 minute, followed by 25 cycles of denaturation at 96°C for 10 seconds, annealing at 50°C for 5 seconds, followed by an extension at 60°C for 2 minutes, then it was held at 4°C.

Table 2.2: List of materials and reaction recipe used in each sequencing reaction.

Contents	**Final concentration**	**1x Reaction (ul)**
Big Dye Terminator	*2.5X*	*1 ul*
Big Dye Buffer	*5X*	*3.5 ul*
Forward/Reverse primer	*5 pmole/ul*	*2 ul*
DNA Template	*3-10 ng/ul*	*2 ul*
D.W	*-*	*11.5 ul*
Total Volume Mix	*20 ul*	

After the sequencing reaction amplification, the sequenced PCR products were purified using the Ethanol/EDTA precipitation method. Initially, 5 µl of freshly prepared 125 mM EDTA from a 5 mM stock was added to each sequencing PCR reaction and thoroughly mixed by continuous pipetting. This step is critical to prevent EDTA from interfering with subsequent processes. Afterward, 60 µl of 100% cold ethanol was added using a multi-channel pipette. Then the plate was sealed with UltraClear sealing film (Axygen, Cat# UC-500), vortexed, and then centrifuged at 2227X G for 30 minutes at 4°C. Following this, the plate was overturned onto a paper towel to discard the supernatant, taking care not to discard the potentially invisible DNA pellet.

The plate was then centrifuged in the inverted position at 2227X G for 5 seconds. Then, 60 µl of 80% pre-cooled ethanol was similarly added using a multi-channel pipette. The plate was sealed, vortexed for at least 1 minute, and centrifuged at 1600X G for 15 minutes at 4°C. Subsequently, it was inverted on a paper towel and centrifuged for 1 minute at 1600X G. The plate was kept in the dark at room temperature for 20 minutes to facilitate more effective ethanol evaporation. After the incubation, 10 µl of HiDi Formamide (Applied Biosystems, Cat# 4311320) was added to each well. The plate was then sealed with a septa mat and briefly centrifuged for 1 minute. After that, the plate was incubated on a hot plate at 95°C for 3 minutes to denature the DNA, followed by cooling on ice for another 3 minutes. Finally, the samples were loaded, and capillary electrophoresis was performed on the 3500 Genetic Analyzer machine from Applied Biosystems to commence the run. Data was analyzed using Sequencing Analysis Software 6.

2.1.8 RNA extraction:

Two to three 3mL peripheral blood samples were collected from participants into EDTA tubes (BioTech, Cat# XLPA-E3K3) and immediately placed on ice. This immediate cooling is a safety measure to prevent the blood from clotting and ensure the integrity of RNA. Instantly after sample collection, the EDTA tubes were centrifuged for 10 minutes at 4°C, with acceleration set to 9 and de-acceleration set to 2 at 400X G to separate the plasma layer, which was then discarded using a transfer pipette. The remaining layer, or buffy coat, containing about 500 ul of red blood cells, was transferred with a sterile pipette into an in house cold, sterile RBC lysis solution in a 50 ml conical tube.

The RBCs lysis solution was prepared as follows; 8.33g of the Ammoium Cloride NH_4Cl (Sigma-Aldrich, Cat# A9434-1KG) was dissolved with 1g Potassium bicarbonate $KHCO_3$ (Sigma-Aldrich, Cat # 237205-500G) in pre-cooled 800 ml distal water to reach a PH of 7.4. Then, 2 mL of 0.5M EDTA was added to the solution, followed by distilled water to bring the total volume to 1000 mL. This solution, known as the RBC lysis solution, is designed to break down the red blood cells, leaving the white blood cells intact for further analysis.
After the samples were vortexed and left on ice for 15-20 minutes, the tubes were centrifuged for 10 minutes at 1800X RPM at 4°C. The supernatant was gently decanted, and care was taken to ensure that the cell pellet remained intact at the bottom of the tube. The buffy coat from each sample was then washed with 5 ml of cold DPBS and centrifuged again for 10 minutes. Finally, 1ml of Trizol (Invitrogen, Cat# 15596018) a ready-to-use reagent that consists of Guanidine isothiocyanate, Phenol, 8-hydroxyquinoline, and β-mercaptoethanol was added to each sample, and the samples were homogenized using an 18Gx1.5 hypodermic needles (Romed holland, Cat# NLD-18GX1.5) with a 10 ml Sterile Disposable Syringes (Medic-pro, Cat# 202306). The lysed cells were then stored at -20C until used. The frozen samples were thawed for 5 minutes at room temperature to ensure complete dissociation of the nucleoprotein complex. Subsequently, 200 µL of chloroform (DAEJUNG, Cat# 2548-4400) was added to each 1 ml TRIzol tube and vortexed for 15 seconds. The samples were then incubated at room temperature for 3 minutes and centrifuged at 12,000X G for 15 minutes at 4°C.

Following centrifugation, the mixture was separated into three layers: a lower pink organic layer containing proteins, an interphase layer containing DNA, and an upper aqueous phase containing RNA. The upper aqueous phase was transferred to a new Eppendorf tube using a disposable transfer pipette. To precipitate the RNA, 500 µL of isopropanol (Iso-Propyl alcohol) (SDFCL, Cat# F12A/0112/1206/31) was added to the aqueous phase. The tubes were mixed by inverting them several times and then centrifuged at 12,000X G for 10 minutes at 4°C. The supernatant was then poured off, leaving a small whitish pellet at the bottom of the tube, which contained the RNA. The RNA pellet was washed by adding 1 mL of 75% cold ethanol and then centrifuged at 7500X G for 5 minutes at 4°C, after which the supernatant was discarded to eliminate the ethanol. This process was repeated twice. The samples were then allowed to dry at room temperature and kept in an inverted position on a Kimtech Science™ Kimwipes®, by Kimberly-Clark, (Cat#34120) for 10 minutes to allow the ethanol to evaporate completely.

Alternatively, the remaining supernatant was carefully removed using a 20 µL pipette, taking care not to disturb the RNA pellet. Finally, the RNA was suspended in molecular-grade water (Sartorius, Cat# 01-869-1A) and incubated at 56°C for 10 minutes. After incubation, the samples were placed directly on ice to measure the RNA concentrations. The nanodrop 2000c Spectrophotometer by Thermo-Scientific was used to assess the quality and concentration of the extracted RNA.

2.1.9 Ethanol Precipitation of RNA:

After the RNA extraction, it was observed that some of the samples had a 260/230 ratio below 2, indicating a high concentration of salts and carbohydrates that could interfere with PCR. To address this issue, ethanol precipitation was performed on these RNA samples. RNA precipitation was carried out by adding 0.1 volumes of 3M Sodium Acetate with a pH of 5.2 (Thermo-Scientific, Cat# R1181) and 2.5 volumes of Ethanol absolute (Dehydrated) (Bio-Lab, Cat# 000525052100). The sample was thoroughly mixed and then chilled for one hour at –80°C. Subsequently, the samples were immediately placed in the centrifuge at 12000X G. After discarding the supernatant, pre-cooled 75% ethanol was added to each sample, which was then vortexed, and centrifuged at 7500X g for 5 minutes. The samples were then allowed to dry at room temperature and placed in an inverted position on a Kim wipe for 10 minutes to facilitate complete evaporation of ethanol. Finally, the RNA was suspended in molecular-grade water (Sartorius, Cat# 01-869-1A) and incubated at 56°C for 10 minutes.

The quality and concentration of the RNA were reassessed using the Nanodrop 2000c Spectrophotometer by Thermo-Scientific.

2.1.10 cDNA synthesis:

A DNA template is necessary for real-time PCR amplification, as it is incompatible with an RNA template. For this purpose, the Maxima First Strand cDNA Synthesis Kit for RT-qPCR (Thermo Scientific Cat#: K1642) was used to create the cDNA entry library. This kit contains

an RNase inhibitor and utilizes a random hexamer primer to initiate reverse transcriptase (RT) binding.

Maxima's reagent, the RT buffer (5X) (Thermo Scientific, Cat#: R1362), was thoroughly mixed with a gentle vortex and then briefly centrifuged after complete thawing in a clean room. The mixture was then prepared, taking into account the number of samples plus the NRT sample (No RNA template). The NRT sample, used to confirm the absence of contamination, contains only the mixture and molecular-grade water (Sartorius, Cat# 01-869-1A) with no RNA template. The enzyme was kept chilled on ice throughout the preparation process to maintain stability and activity. The specific amounts of each reagent required for the cDNA reaction mix are detailed in (**Table 2.3)**.

Table 2.3: list of materials and recipe utilized in the reverse transcriptase (RT) reaction.

cDNA reaction mix	**1x Reaction (ul)**
RT buffer (5X)	*4 ul*
Maxima Enzyme mix	*2 ul*
RNA *Template (*1000 *ng)*	*Up to 14 ul*
Total Volume Mix	*20 ul*

Following the preparation of the mix, 6 µl was carefully distributed into 0.2 mL PCR microtubes (Axygen, Cat# PCR-0208-C). Subsequently, 1000 ng of each chilled RNA sample was added to the mixture in a separate room. Molecular-grade water (Sartorius, Cat# 01-869-1A) was then added to adjust the volumes of each mix to 20 µl. The reaction was then carried out in a C1000 Touch™ PCR thermal cycler from BIO-RAD using the following program:

The reaction was incubated at 25°C for 10 minutes, followed by 25 minutes at 50°C. The temperature was then raised to 65°C for 10 minutes to deal with CG-rich RNA templates and prevent the existence of secondary structures. Finally, the reaction was terminated at 85°C for 5 minutes, followed by a hold at 4°C. Finally, the cDNA product was fully prepared and ready to be used in the PCR reaction.

3. Chapter Three

3.1 Results

3.1.1 Variant pathogenicity assessment using in silico analysis:

The conservation of amino acids provides insight into their significance for protein function. To analyse this, the protein sequences of OSTM1 from different species were aligned using two multiple sequence alignment tools: Clustal Omega (Clustal Omega < EMBL-EBI) (**Figure 3.1**) and Cobalt (COBALT: Multiple Alignment Tool (nih.gov)) (**Figure 3.2**). The analysis revealed that Valine residues are not highly conserved.

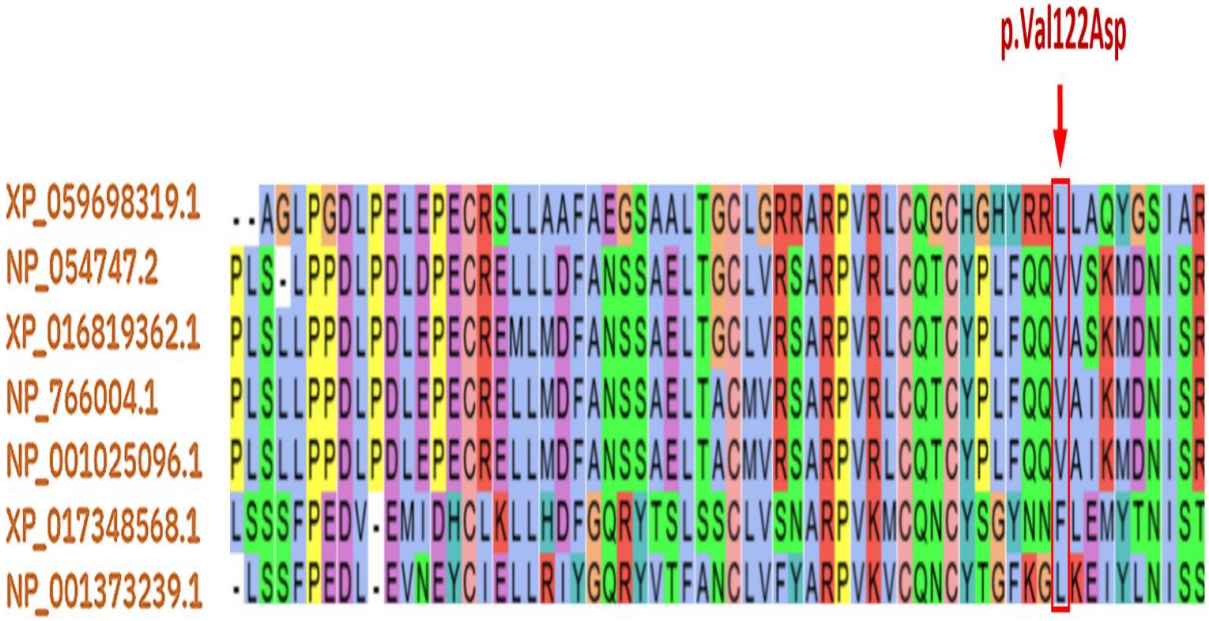

Figure 3.1: OSTM1 protein conservation analysis. Protein sequence alignment by Clustal Omega of OSTM1 protein sequence flanking Val122Asp variant site obtained from different species. The identified variant site is denoted by an arrow.

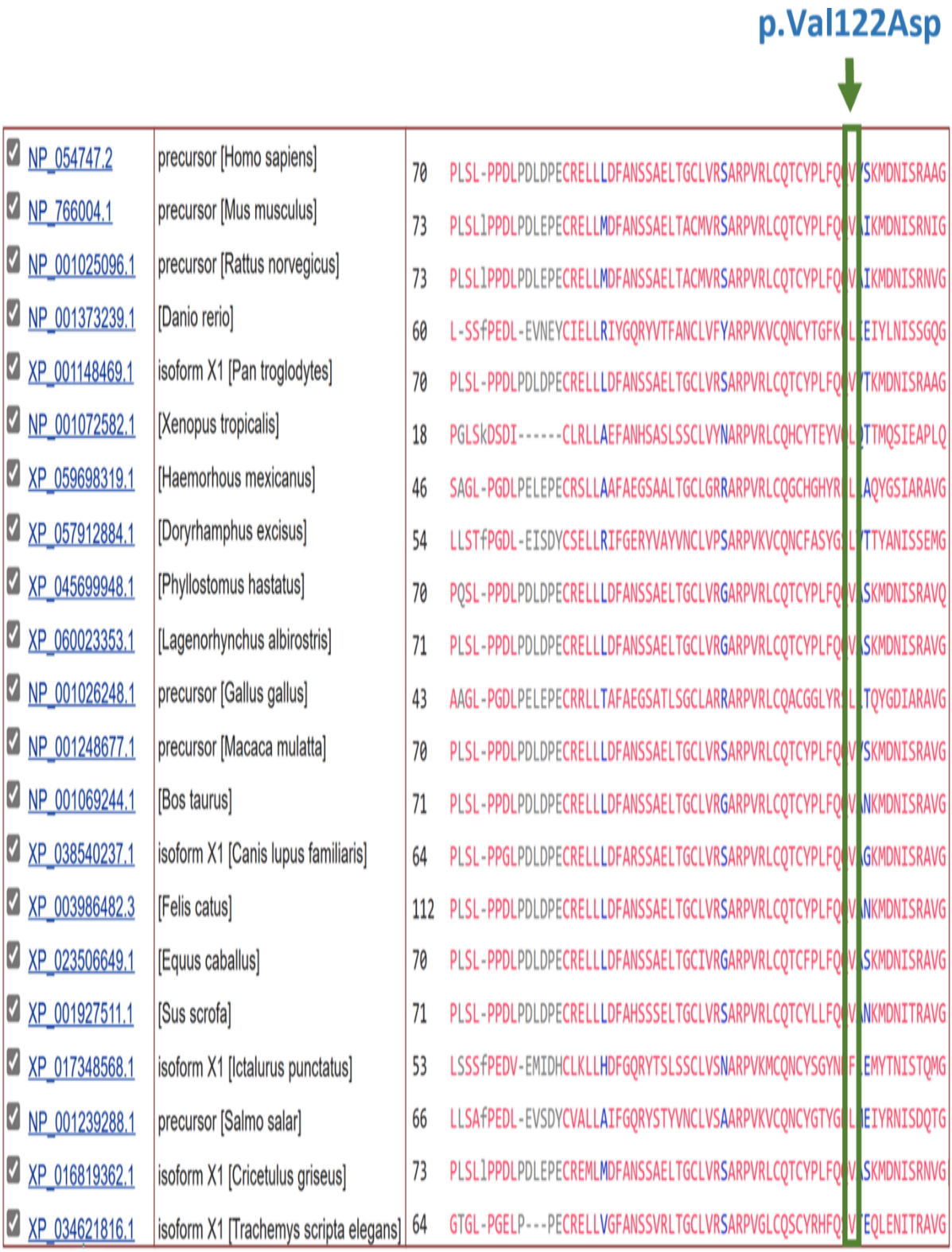

Figure 3.2: Conservation analysis of OSTM1 Val122Asp variant site. Multiple sequence alignment by Cobalt of part of OSTM1 protein sequence from different species. The identified varient is marked with an arrow, indicating that the Valine residues are not highly conserved.

Moreover, the variant's pathogenicity was tested using several web-based tools, including; MutationTaster at http://www.mutationtaster.org/, PolyPhen-2 at http://genetics.bwh.harvard.edu/pph2/, Pathogenicity Calculator https://seq.genomize.com/pathogenicity_calculator/ and Clinvar at https://www.ncbi.nlm.nih.gov/clinvar/.

In addition, we used the AlphaMissence server (J. Cheng et al., 2023), which utilizes related protein sequences and protein structure to estimate pathogenicity. The identified variant Val122Asp is predicted to be "likely pathogenic" or "Unsertain significant", and "probably damging" while the other variant Gly36 Gly was predicted to be "benign" or "Unsertain significant". Alphafold-3 (Abramson, J et al. Accurate structure prediction of biomolecular interactions with AlphaFold 3. Nature (2024), https://www.nature.com/articles/s41586-024-07487-w) was unable to predict structure distortion upon the V122D varient. However, careful structural analysis suggests that the varient of Val122 into Asp would introduce an unsuited polar charge into a hydrophobic core essential for maintaining the fold of the β subunit OSTM1. Asp122 is likely to introduce steric clashes with nearby hydrophobic residues Phe162 and Leu98, and its negative charge could cause electrostatic repulsion with the hydroxyl group of Ser95, see (**Figure 3.3**).

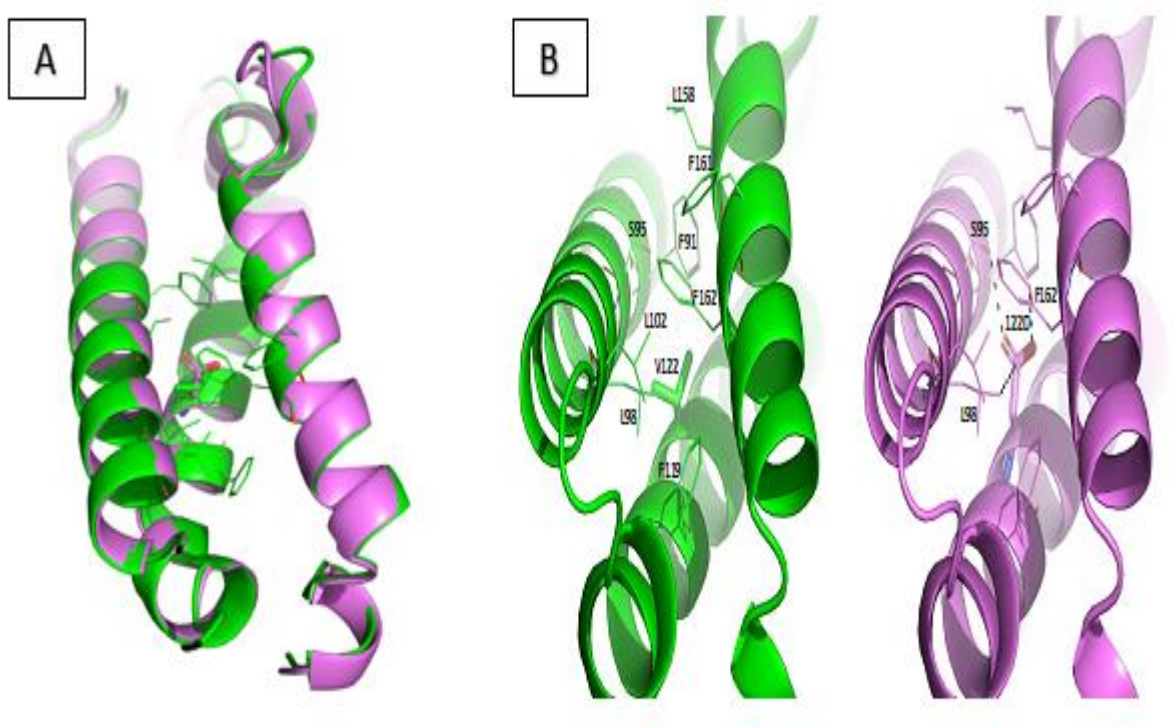

Figure 3.3: Structural analysis of the effect of V122D variant on OSTM1 folding. (A) The Alphafold prediction shows the structure of the β subunit containing V122D in purple, compared to the wild-type structure in green. The structures of V122D and V122 are depicted using sticks, while the hydrophobic core residues are represented with lines. **(B)** In the β subunit of OSMT1, the hydrophobic core including Phe162 and Leu98 residues is not favourable for Asp122 . The dashed lines in the right panel indicate potential steric clash with F162 and L98, or electrostatic repulsion with S95 hydroxyl.

Furthermore-based analysis of this variant (V122D) strongly predicts that it will disrupt the function of OSTM1, specifically its ability to form stable dimers, which are essential for its proper functioning. Since Val122 is located at the center of the hydrophobic core, any impairment in dimer formation negatively impacts OSTM1's association with lysosomal membranes and its ability to bind to and stabilize the CLC-7 see, (**Figure 3.4**) (Zhang et al., 2020).

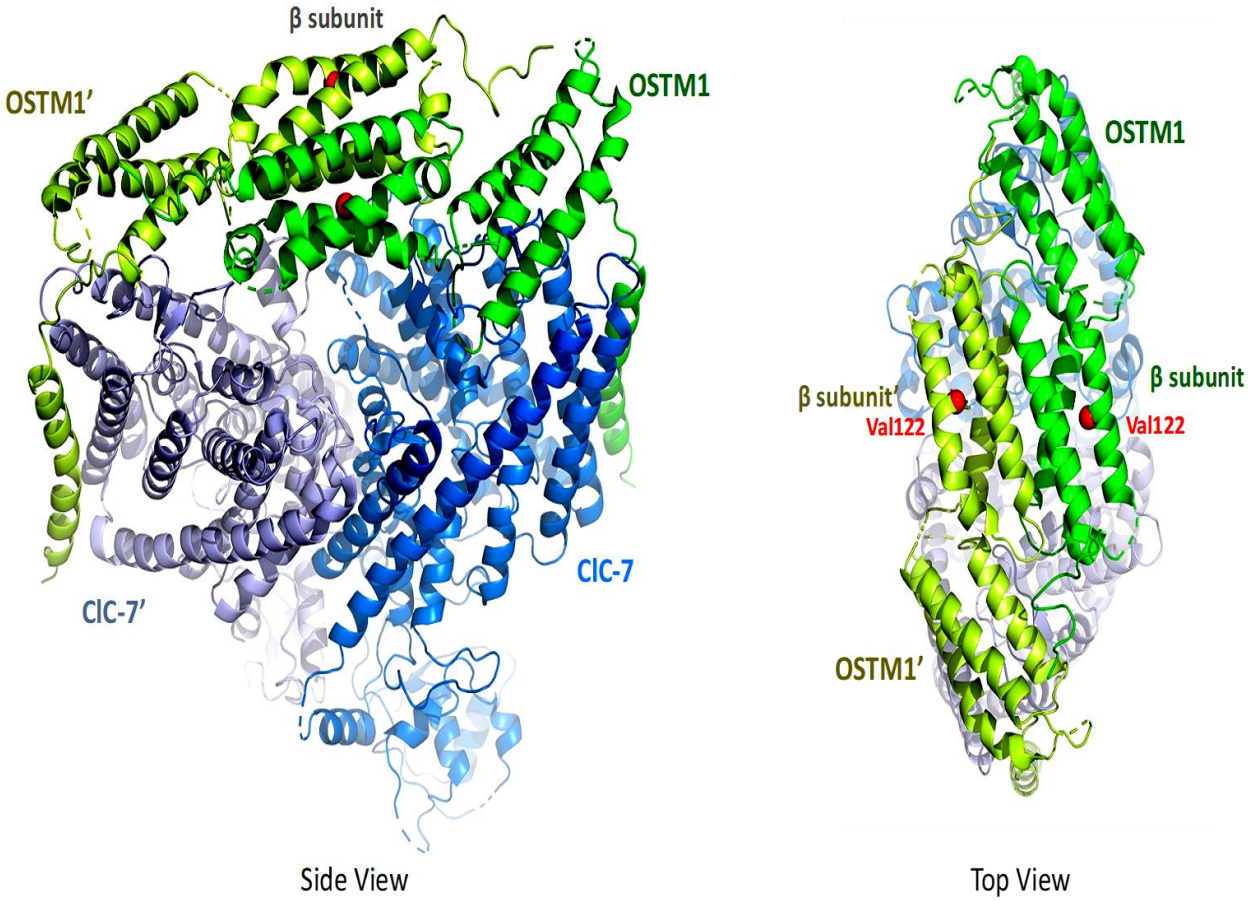

Figure 3.4: Structure of OSTM1-ClC-7 complex (PDB: 7BXU). OSTM1 dimer is shown in green and lime-green. The ClC-7 dimer is shown in blue and light blue. Dimerization of β subunit in OSTM1 is emphasized. Val122 at the center of the hydrophobic core of β subunit is shown with red spheres (Cα).

Additionally, our analysis employed two bioinformatics tools, SPIP and RNA Splicer, to examine the potential effects of the genetic variant c.108 C>T (p.Gly36Gly) on mRNA splicing processes. The results from both SPIP and RNA Splicer suggested the possibility of creating an alternative splice site due to this variant, which could impact normal gene expression. The findings from this analysis are illustrated in (**Figure 3.5**) and (**Figure 3.6**).

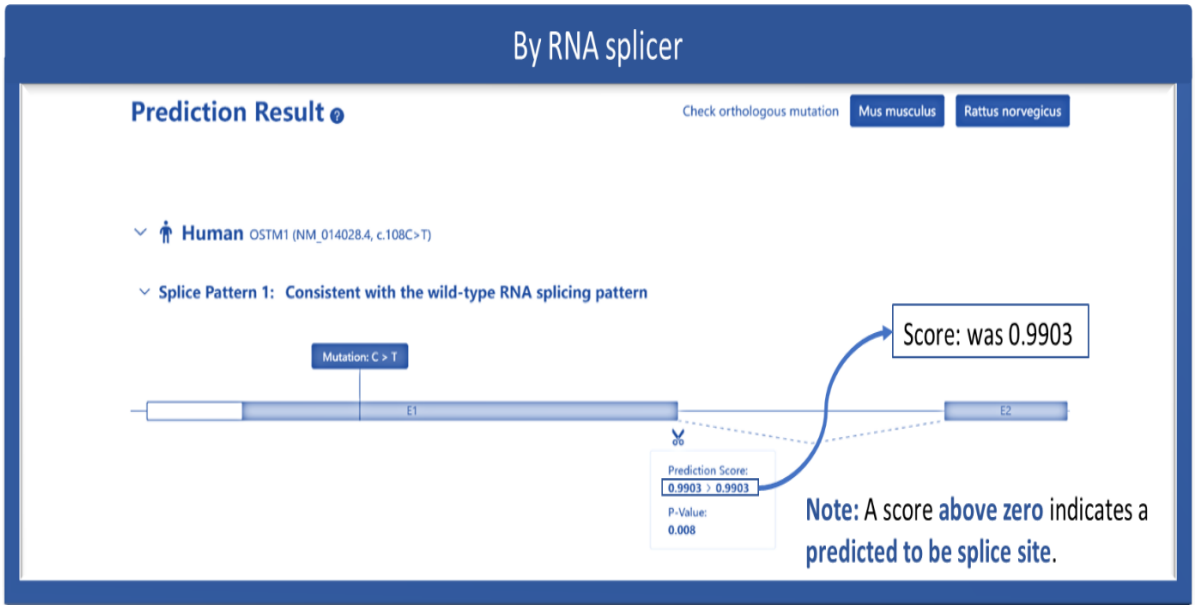

Figure 3.5: Analysis of splicing in the genetic variant (c.108 C>T) by RNA splicer. This tool predicts the effect on splicing and assigned a score of 0.9903, indicating a predicted to be splice site.

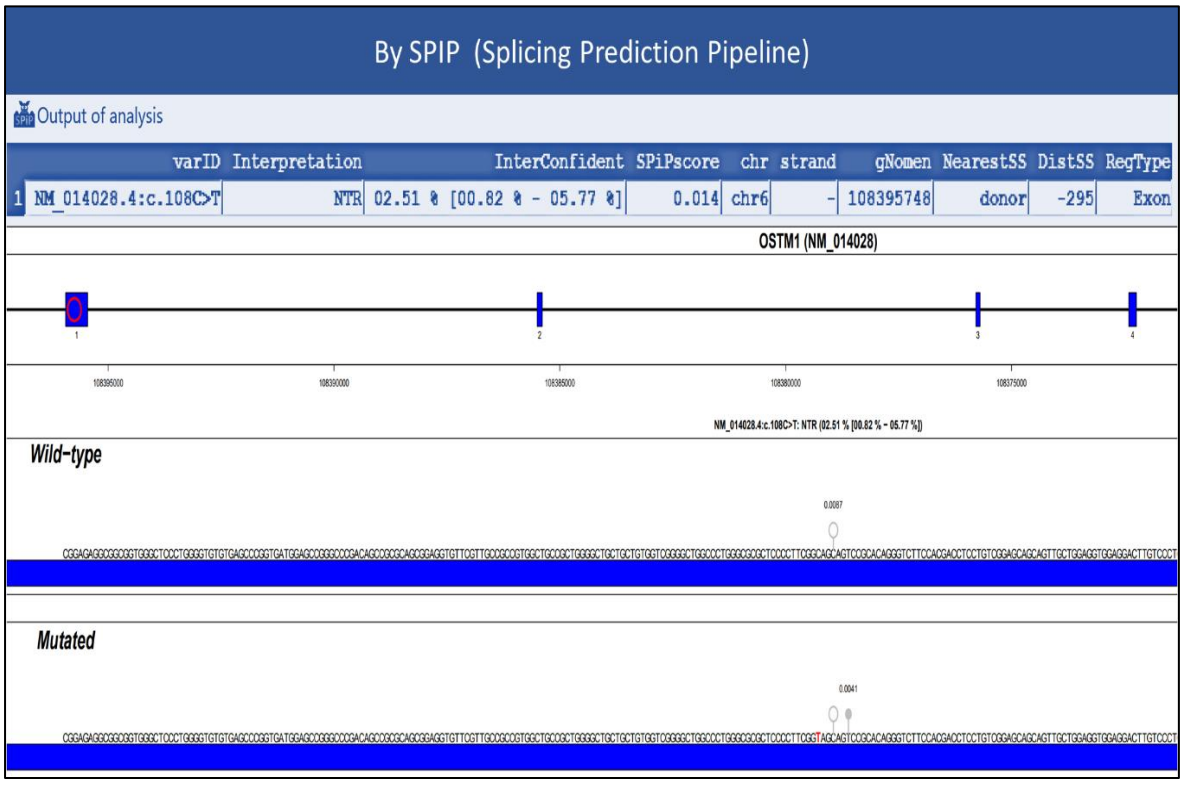

Figure 3.6: Analysis of splicing for the genetic variant (c.108 C>T) was conducted using the SPIP tool. This tool predicts the impact of mutations on splicing. The tool identified two predicted splicing sites following the mutation, with the site having the higher score indicating the location of our variant. Therefore, it is most likely that splicing will occur at this site.

3.1.2 Segregation analysis of Val122Asp and Gly36 Gly:

Segregation was performed using Sanger sequencing to assess the pathogenicity of the two variants of interest. The 496 bp flanking sequence was amplified in thirty-six participants using the primers listed in (**Appendix 7.1, Table 7.1**). This encompasses the two variants of interest in Exon One: the c.365 T>A (Val122Asp) variant and the c.108 C>T (p.Gly36Gly) variant. As depicted in (**Figure 3.7**), The DNA sequences containing both of our variants were amplified.

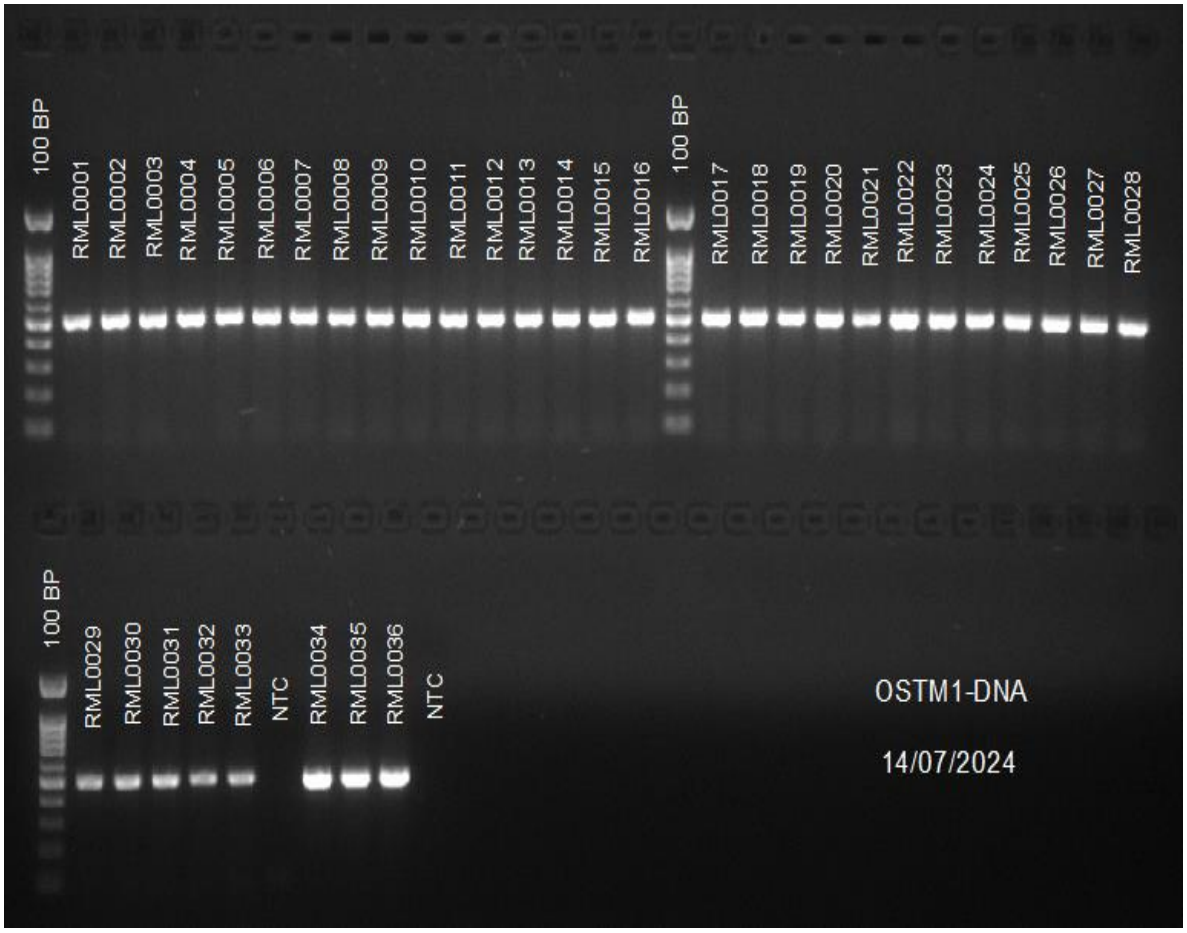

Figure3.7: Agarose gel electrophoresis analysis of OSTM1 PCR products. Gel agarose showing the PCR products flanking exon1 variants.

The Sanger sequencing analysis conducted on thirty-six participants—including four individuals affected by the condition and thirty-two unaffected individuals—provided insights into the genetic variants present within this group. The results indicated that the unaffected parents were carriers of both variants in a heterozygous state, while the affected individuals were homozygous for these two variants. For the first variant, c.365 T>A, affected individuals exhibited a nucleotide substitution in which A replaced T. Similarly, for the second variant, c.108 C>T, there was a nucleotide substitution where T replaced C compared to the wild type, as illustrated in (**Figure 3.8**).

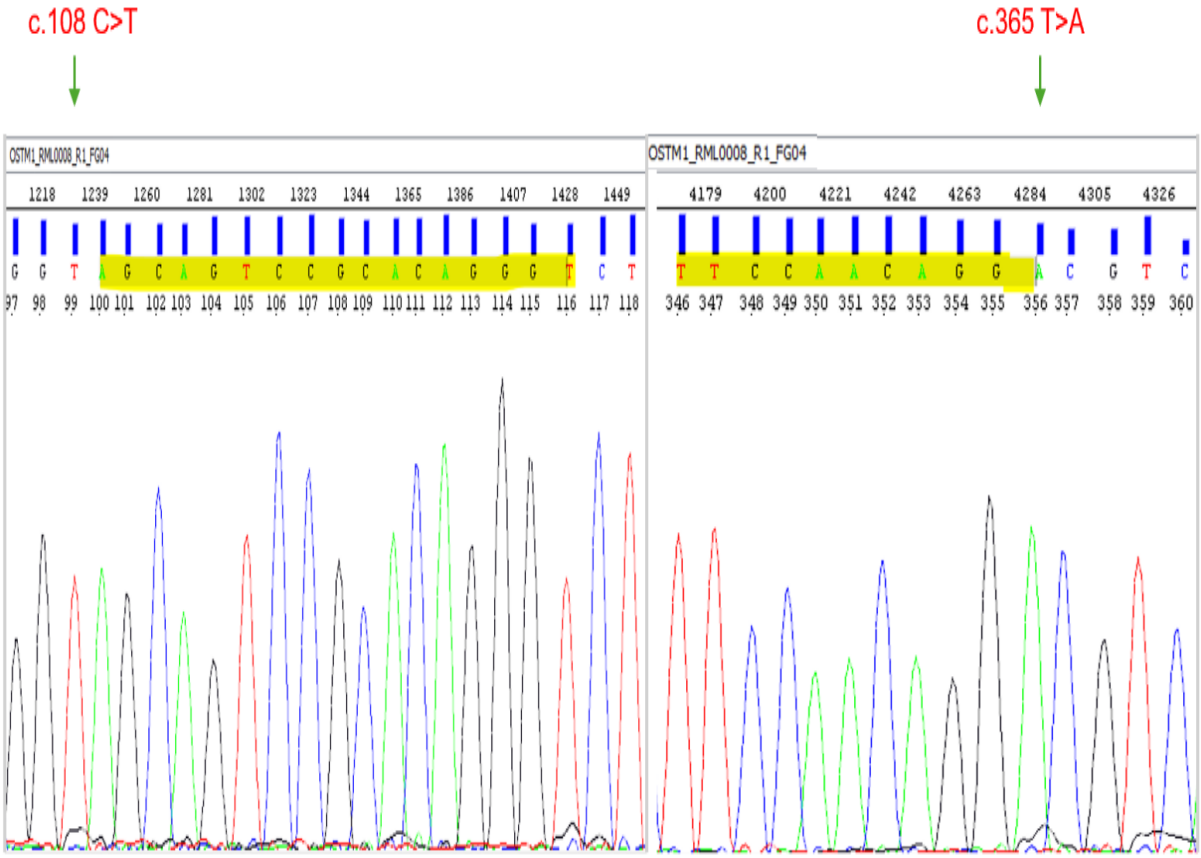

Figure 3.8: Sanger sequencing analysis of OSTM1 variants. The figure depicts the electropherogram of one affected individual who previously had an unknown genotype. As indicated by the arrows, he is homozygous for both variants of interest.

In contrast, genetic testing showed a variety of results among the unaffected siblings of the affected individuals. Some siblings displayed a wild-type genotype, indicating no mutations in the analyzed regions, while others showed a heterozygous state, meaning they carried one copy of the variant and one normal allele (wild type). This inheritance pattern among the siblings suggests a recessive inheritance model, in which both variants must be present in a homozygous state for the phenotype to manifest (**see Appendix 7.2**).

(**Figure 3.9**) displays the electropherograms from the genetic sequences of the parents and their affected child, alongside those from the wild-type grandfather and the heterozygous grandmother. This comparative analysis indicated a recessive inheritance pattern for the identified variants, suggesting that both copies of the variant must be present for the phenotype to appear. Furthermore, it was determined that these variants are in a coupling (or cis) configuration, meaning they are located close together on the same chromosome. This further supports the notion of a recessive trait within the family's genetic background.

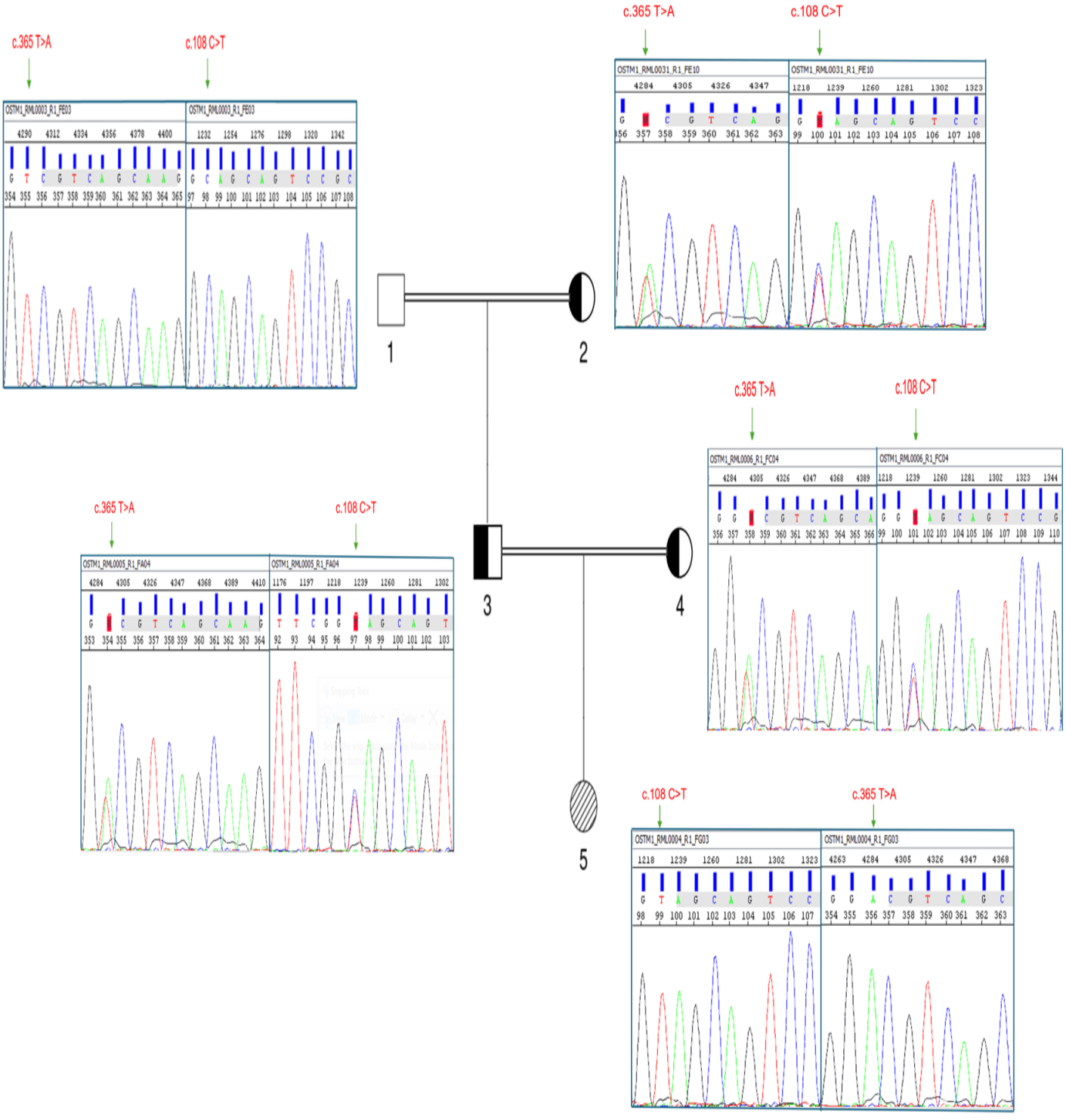

Figure 3.9: Genotype-Phenotype Electropherogram comparison. A comparison of electropherograms between the affected patient, his heterozygous parents, and paternal grandparents. The grandmother is a carrier for both variants, while the grandfather is of the wild type. In the pedigree, squares represent males, and circles represent females. Half-shaded symbols signify carriers, while multiple diagonal lines represent affected individuals.

3.1.3 Functional assessment of c.108 C>T variant pathogenicity:

The c.108C>T variant is classified as a synonymous variant, meaning it does not alter the protein's amino acid sequence; however, recent predictions suggest that it may interfere with normal splicing processes by creating an unintended donor splicing site. To investigate this prediction, RNA splicing analysis was performed using RNA obtained from the white blood cells of individuals carrying the c.108 C>T (p.Gly36Gly) variant, as well as from individuals who are wild type and heterozygous for this variant. For the analysis, complementary DNA (cDNA) was amplified using a GoTaq master mix with specific primers designed to flank exons one and two of the target gene (**refer to Appendix 7.1, Table 7.2 for primer details**). If the c.108 C>T variant indeed induced alternative splicing, we would anticipate the generation of a 108 bp PCR product, which would indicate a partial deletion of exon 1.

The analysis involved several participants identified as RML00001, RML0033, and RML0020, who were categorized as wild types for the p.Gly36Gly variant. Additionally, participants labeled as RML0004, RML0008, RML0021, and RML0022 were found to be homozygous for the p.Gly36Gly variant, while those marked as RML0028, RML0023, and RML0030 were heterozygous for the same variant.

Upon analysis, all participants displayed two distinct bands—400 bp and 147 bp—in both affected and unaffected individuals. Notably, these bands were consistently present in individuals carrying the variant as well as in those classified as wild-type, as illustrated in (**Figure 3.10**). It is important to highlight that the 108 bp band was absent in every participant, regardless of their genetic variant classification.

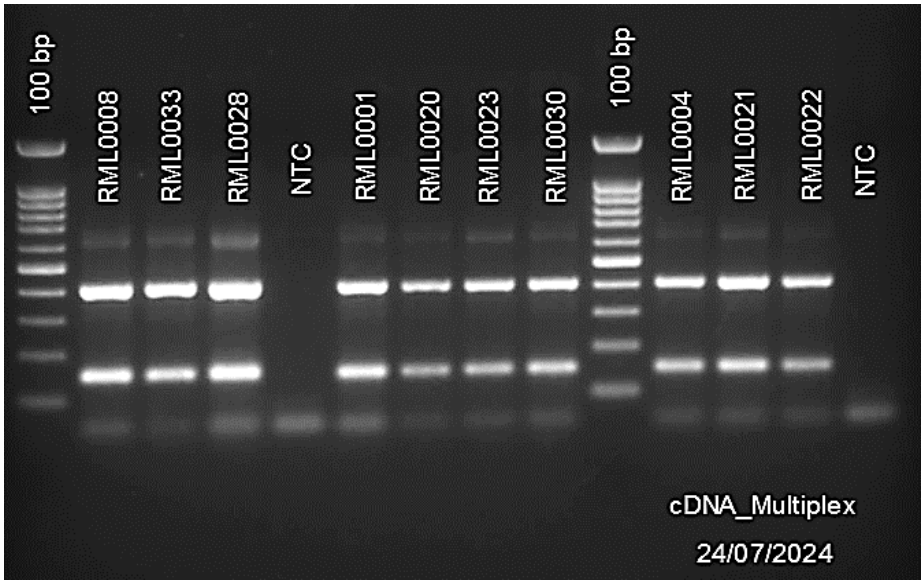

Figure 3.10: Impact of the c.108C>T variant on OSTM1 RNA splicing analysis. Gel electrophoresis was performed on PCR products generated by primers that flank the c.108C>T

variant. The results show two bands in the PCR products for all participants, irrespective of their genetic phenotype. This finding refutes the possibility of a new splicing site at position 108.

These findings suggest that, contrary to previous assumptions, the p.Gly36Gly variant does not create a splicing site, as initially speculated. This insight contributes to a better understanding of the genetic implications of the p.Gly36Gly variant in relation to splicing activity.

4. Chapter Four

4.1 Discussion

This study utilized Whole Exome Sequencing (WES) results from three affected patients to investigate osteopetrosis in Palestinian families, with the goal of achieving a precise genetic diagnosis. The findings revealed two significant homozygous variants located in Exon 1 of the OSTM1 gene, which is known to be associated with infantile autosomal recessive osteopetrosis—a rare and severe bone disorder characterized by excessive bone accumulation, resulting in increased fragility and a higher risk of fractures. Clinical assessments of the affected patients, which included thorough medical histories and detailed physical examinations, supported the WES results. Additionally, radiological evaluations through X-rays highlighted bone changes typical of osteopetrosis, further reinforcing the genetic findings. Notably, these two variants have not been previously documented as pathogenic in scientific literature, nor have they been studied at a molecular level in earlier research. This study desired to understand the genetic causes of osteopetrosis in these families and demonstrates how the OSTM1 gene influences bone health.

For the first variant in exon one c.365 T>A (p.Val122Asp), a comparison of OSTM1 amino acid sequences from various species indicates that p.Val122 is not well-conserved (Figure 13 and Figure 14). Despite valine and aspartic acid being dissimilar amino acids, the lack of high conservation suggests that p.Val122Asp may represent a neutral variant. The second variant in exon1, c.108 C>T (p.Gly36Gly), is a silent mutation; GGC and GGT are both codons for glycine. However, the c.108 C>T transition was suspected to create a new donor splice site (GT), resulting in aberrant mRNA processing. Mahmoud A. and his colleagues also emphasized these two points in their 2013 findings (Mahmoud et al., 2013).

Segregation analysis of OSTM1 variants in affected Palestinian families revealed that both parents carried the c.108 C>T and c.365 T>A variants in a heterozygous state. The siblings of the affected participant were either heterozygous or wild type. This suggests that the affected patients inherited the condition in an autosomal recessive manner from their parents, and one

or both of the identified variants likely contributed to the development of the disease. Since mutations in the OSTM1 gene are known to cause osteopetrosis, our research project aimed to determine which of the two variants (c.365 T>A and c.108 C>T) in the OSTM1 gene is pathogenic and leads to osteopetrosis.

Among our study subjects, 21 of 36 unaffected individuals (approximately 59%) were heterozygous for both variants. In contrast, four affected individuals (about 11%) were homozygous for both variants, while 10 unaffected individuals (about 28%) were homozygous for the wild-type variants. Upon further analysis, we concluded that the second variant, c.108C>T (p.Gly36Gly), does not create a functional splice site in the RNA as previously believed. Therefore, we determined that the c.108C>T (p.Gly36Gly) variant is neutral.

Unfortunately, no functional studies are available on the two variants or nearby locations. However, our structural analysis indicates that Val122 plays a crucial role in the ancillary β subunit of the OSTM1 transmembrane domain. This residue is strategically positioned at the center of the hydrophobic core and is essential for the functional dimerization of OSTM1, allowing it to interact with the chloride channel CIC-7. The OSTM1-CLC-7 complex is vital for transporting CLC-7 to the ruffled border of osteoclasts, which is necessary for their resorption function.

If the hydrophobic, non-polar Val122 were to be mutated into a polar, hydrophilic Asp residue, it would likely disrupt the hydrophobic core of the β subunit of OSTM1. This could have severe consequences for OSTM1's stability, abundance, and overall function. Specifically, this variant (V122D) is highly predicted to impair OSTM1’s ability to form functional dimers, associate with lysosomal or osteoclast membranes, and bind to and stabilize the chloride channel ClC-7. As a result, it would hinder the stability of the chloride-proton antiporter and its essential role in lysosomal acidification and bone resorption (Vacher et al., 2020).

Additionally, this variant may negatively impact the proper folding of the β subunit of OSTM1, leading also to compromised functional dimerization. This pairing is critical for the capping and stabilization of ClC-7 (Zhang et al., 2020).

It is noteworthy that although the variant p.Val122 is not well-conserved across species, alternative residues such as leucine, phenylalanine, and valine, which may replace valine in some species, possess similar properties. These three amino acids are uncharged and hydrophobic, contrasting with aspartic acid, which is characterized by its negative charge and hydrophilic nature. This difference suggests that the changes observed could be significant and may elucidate why this amino acid alteration disrupts the protein’s function. Conversely, the other amino acids preserved in different species maintain the protein's structure and functionality.

The presence of the p.Val122Asp variant in all affected family members, its likely pathogenic nature in the public database, and its location in the protein, suggest that it may be a pathogenic mutation rather than a neutral variant. Our comprehensive study covers a diverse range of ages, genetic phenotypes, and participants, demonstrating the thoroughness and reliability of our findings. This study can significantly influence future research and is relevant to many individuals, highlighting its significance.

5. Chapter Five

5.1 Conclusion

Our study established a connection between the c.365 T>A mutation and osteopetrosis, a rare genetic disorder characterized by abnormally dense bones. This discovery has significant implications for patient care, but further research is needed to confirm our findings. We determined that the synonymous variant c.365 T>A (p.Val122Asp) is not pathogenic, while the missense mutation c.108C>T (p.Gly36Gly) alters the protein structure, at least according to our computational analysis. Therefore, it is likely that this variant is responsible for the disease. Research like this is crucial for identifying individuals at risk, providing essential patient counseling, and potentially preventing osteopetrosis. Additionally, our findings may offer valuable insights into the genetic mechanisms underlying osteopetrosis, emphasizing the urgent need for further investigation to fully understand and address this condition.

References

- Al-Bari, A. A., , Al Mamun, A., & (2020). Current advances in regulation of bone homeostasis. In (Vol. 2, pp. 668-679).
- Alotaibi, Q., , Dighe, M., & (2021). Managing challenging pain and irritability in OSTM1 mutation-related infantile malignant osteopetrosis. In (Vol. 14, pp. e242498).
- Alotaibi, Q., , Dighe, M., , Aldaihani, S., & (2023). The clinical features of <scp> OSTM1 </scp> -associated malignant infantile osteopetrosis: A retrospective, single-center experience over one decade. In (Vol. 191, pp. 459-468).
- Bollerslev, J., , Andersen, P. E., & (1988). Radiological, biochemical and hereditary evidence of two types of autosomal dominant osteopetrosis. In (Vol. 9, pp. 7-13).
- Boyle, W. J., , Simonet, W. S., , Lacey, D. L., & (2003). Osteoclast differentiation and activation. In (Vol. 423, pp. 337-342).
- Chalhoub, N., , Benachenhou, N., , Rajapurohitam, V., , ... (2003). Grey-lethal mutation induces severe malignant autosomal recessive osteopetrosis in mouse and human. In (Vol. 9, pp. 399-406).
- Chen, X., , Zhang, K., , Hock, J., , ... (2016). Enhanced but hypofunctional osteoclastogenesis in an autosomal dominant osteopetrosis type II case carrying a c.1856C>T mutation in CLCN7. In (Vol. 4, pp. 16035).
- Cheng, C.-H., , Chen, L.-R., , Chen, K.-H., & (2022). Osteoporosis Due to Hormone Imbalance: An Overview of the Effects of Estrogen Deficiency and Glucocorticoid Overuse on Bone Turnover. In (Vol. 23).
- Cheng, J., Novati, G., Pan, J., Bycroft, C., Žemgulytė, A., Applebaum, T., . . . Avsec, Ž. (2023). Accurate proteome-wide missense variant effect prediction with AlphaMissense. *Science, 381*(6664), eadg7492. doi:doi:10.1126/science.adg7492
- Hengel, H., , Buchert, R., , Sturm, M., , ... (2020). First-line exome sequencing in Palestinian and Israeli Arabs with neurological disorders is efficient and facilitates disease gene discovery. In (Vol. 28, pp. 1034-1043).
- Jung-Min, K., , Lin, C., , Stavre, Z., , ... (2020). Osteoblast-Osteoclast Communication and Bone Homeostasis. In (Vol. 9, pp. 2073).
- Lange, P. F., , Wartosch, L., , Jentsch, T. J., , ... (2006). ClC-7 requires Ostm1 as a β-subunit to support bone resorption and lysosomal function. In (Vol. 440, pp. 220-223).
- Mahmoud, A. A., , Abdullah, A. J., , Eissa, F., & (2013). Infantile osteopetrosis, craniosynostosis, and Chiari malformation type I with novel OSTEM1 mutation. In (Vol. 8, pp. 34).
- Mulari, M. T. K., , Zhao, H., , Lakkakorpi, P. T., , ... (2003). Osteoclast Ruffled Border Has Distinct Subdomains for Secretion and Degraded Matrix Uptake. In (Vol. 4, pp. 113-125).
- Palagano, E., , Menale, C., , Sobacchi, C., , ... (2018). Genetics of Osteopetrosis. In (Vol. 16, pp. 13-25).
- Pandruvada, S. N. M., , Beauregard, J., , Benjannet, S., , ... (2016). Role of Ostm1 Cytosolic Complex with Kinesin 5B in Intracellular Dispersion and Trafficking. In (Vol. 36, pp. 507-521).
- Pangrazio, A., , Poliani, P. L., , Megarbane, A., , ... (2006). Mutations in OSTM1 (Grey Lethal) Define a Particularly Severe Form of Autosomal Recessive Osteopetrosis With Neural Involvement. In (Vol. 21, pp. 1098-1105).

- Pata, M., , Yousefi Behzadi, P., , Vacher, J., & (2021). Expression pattern of the V5-Ostm1 protein in bacterial artificial chromosome transgenic mice. In (Vol. 59).
- Penna, S., , Villa, A., , Capo, V., & (2021). Autosomal recessive osteopetrosis: mechanisms and treatments. In (Vol. 14).
- Pillai, N. R., , Aggarwal, A., , Orchard, P., & (2022). Phenotype-autosomal recessive osteopetrosis. In (Vol. 165, pp. 116577).
- Ponzetti, M., , Rucci, N., & (2021). Osteoblast Differentiation and Signaling: Established Concepts and Emerging Topics. In (Vol. 22, pp. 6651).
- Pusch, M., , Zifarelli, G., & (2021). Large transient capacitive currents in wild-type lysosomal Cl−/H+ antiporter ClC-7 and residual transport activity in the proton glutamate mutant E312A. In (Vol. 153).
- Ramírez, A., , Faupel, J., , Goebel, I., , ... (2004). Identification of a novel mutation in the coding region of the grey-lethal gene OSTM1 in human malignant infantile osteopetrosis. In (Vol. 23, pp. 471-476).
- Schrecker, M., Korobenko, J., & Hite, R. K. (2020). Cryo-EM structure of the lysosomal chloride-proton exchanger CLC-7 in complex with OSTM1. *eLife*, *9*, e59555. doi:10.7554/eLife.59555
- Shah, G. N., , Bonapace, G., , Hu, P. Y., , ... (2004). Carbonic anhydrase II deficiency syndrome (osteopetrosis with renal tubular acidosis and brain calcification): Novel mutations in CA2 identified by direct sequencing expand the opportunity for genotype-phenotype correlation. In (Vol. 24, pp. 272-272).
- Sobacchi, C., , Schulz, A., , Coxon, F. P., , ... (2013). Osteopetrosis: genetics, treatment and new insights into osteoclast function. In (Vol. 9, pp. 522-536).
- Souraty, N., , Noun, P., , Djambas-Khayat, C., , ... (2007). Molecular study of six families originating from the Middle-East and presenting with autosomal recessive osteopetrosis. In (Vol. 50, pp. 188-199).
- Spinnato, P., , Pedrini, E., , Petrera, M. R., , ... (2022). Spectrum of Skeletal Imaging Features in Osteopetrosis: Inheritance Pattern and Radiological Associations. In (Vol. 13, pp. 1965).
- Takegahara, N., , Kim, H., , Choi, Y., & (2024). Unraveling the intricacies of osteoclast differentiation and maturation: insight into novel therapeutic strategies for bone-destructive diseases. In (Vol. 56, pp. 264-272).
- Titorencu, I., , Pruna, V., , Jinga, V. V., , ... (2014). Osteoblast ontogeny and implications for bone pathology: an overview. In (Vol. 355, pp. 23-33).
- Udagawa, N., , Koide, M., , Nakamura, M., , ... (2021). Osteoclast differentiation by RANKL and OPG signaling pathways. In (Vol. 39, pp. 19-26).
- Vacher, J. (2022). OSTM1 pleiotropic roles from osteopetrosis to neurodegeneration. In (Vol. 163, pp. 116505).
- Vacher, J., , Bruccoleri, M., , Pata, M., & (2020). Ostm1 from Mouse to Human: Insights into Osteoclast Maturation. In (Vol. 21, pp. 5600).
- Wu, C. C., , Econs, M. J., , DiMeglio, L. A., , ... (2017). Diagnosis and Management of Osteopetrosis: Consensus Guidelines From the Osteopetrosis Working Group. In (Vol. 102, pp. 3111-3123).
- Zhang, S., Liu, Y., Zhang, B., Zhou, J., Li, T., Liu, Z., . . . Yang, M. (2020). Molecular insights into the human CLC-7/Ostm1 transporter. *Science Advances, 6*(33), eabb4747. doi:doi:10.1126/sciadv.abb4747

Appendices

Appendix 7.1

Primer sequences:

Table 7.1: Table: Primers sequences used for Sanger sequencing:

Primer Name	Ref seq.	Sequence
OSTM_ seq-F	NG_007262.1	5’-gtgtgtgagcccggtgat
OSTM _seq-R	NG_007262.1	5’-ccagcgctgaccatcattac

Table 7.2: Table: Primers sequences used for RNA analysis:

Primer Name	Ref seq.	Sequence
OSTM_ Gly36Gly _RNA-F	NM_014028	5’-gaggtgttcgttgccgcc
OSTM_RNA _EX1-R	NM_014028	5’-gacaagtcctccacctccag
OSTM_RNA_EX2-R	NM_014028	5’-ggcacaactctgactctctg

Appendix 7.2

Participant genotypic results for the two variants are represented in the table below.

Number	Paticipant	Gender	Age	Phenotype	p.Val122Asp / c.365 T>A	p.Gly36Gly / c.108 C>T
RML0001	Aunty of K/Mother & B/Father	F	47	Unaffected	Wild type	Wild type
RML0002	Aunkle of B/father & K/mother	M	34	Unaffected	Wild type	Wild type
RML0003	Grandfather of B/Father & K/Mother	M	74	Unaffected	Wild type	Wild type
RML0004	B	F	6 months	Affected	Homozygous (A)	Homozygous (T)
RML0005	Father of B & Unkle of K/Mother	M	45	Unaffected	Heterozygous (A/T)	Heterozygous (C/T)
RML0006	Mother of B	F	36	Unaffected	Heterozygous (A/T)	Heterozygous (C/T)
RML0007	Mother of K & Aunty of B	F	40	Unaffected	Heterozygous (A/T)	Heterozygous (C/T)
RML0008	A	M	12	Affected	Homozygous (A)	Homozygous (T)
RML0009	Father of A	M	43	Unaffected	Heterozygous (A/T)	Heterozygous (C/T)
RML0010	Mother of A	F	38	Unaffected	Heterozygous (A/T)	Heterozygous (C/T)
RML0011	Mother of C	F	27	Unaffected	Heterozygous (A/T)	Heterozygous (C/T)
RML0012	Father of C	M	30	Unaffected	Heterozygous (A/T)	Heterozygous (C/T)
RML0013	Grandfather of C/Father	M	53	Unaffected	Heterozygous (A/T)	Heterozygous (C/T)
RML0014	Brother of C	M	5 and half	Unaffected	Heterozygous (A/T)	Heterozygous (C/T)
RML0015	Brother of C	M	1 and 2 months	Unaffected	Wild type	Wild type
RML0016	Uncle of C/Father	M	27	Unaffected	Heterozygous (A/T)	Heterozygous (C/T)
RML0017	Brother of A & Cousin of K/Mother	M	10	Unaffected	Heterozygous (A/T)	Heterozygous (C/T)
RML0018	Brother of A & Cousin of K/Mother	M	18	Unaffected	Wild type	Wild type
RML0019	Aunkle of B/father & K/mother	M	40	Unaffected	Heterozygous (A/T)	Heterozygous (C/T)
RML0020	Cousin of K & B/ Father	M	9	Unaffected	Wild type	Wild type
RML0021	K	M	4	Affected	Homozygous (A)	Homozygous (T)
RML0022	C	F	2 and a half	Affected	Homozygous (A)	Homozygous (T)
RML0023	Aunty of B/Mother	F	44	Unaffected	Heterozygous (A/T)	Heterozygous (C/T)
RML0024	Grandmother of B/Mother	F	65	Unaffected	Wild type	Wild type
RML0025	Grandmother of C/Father	F	55	Unaffected	Wild type	Wild type
RML0026	Brother of B and Cousin of K/Father	M	6	Unaffected	Heterozygous (A/T)	Heterozygous (C/T)
RML0027	Brother of B and Cousin of K/Father	M	17	Unaffected	Heterozygous (A/T)	Heterozygous (C/T)
RML0028	Sister of B and Cousin of K/Father	F	11	Unaffected	Heterozygous (A/T)	Heterozygous (C/T)
RML0029	Cousin of K and B/ Father	F	12	Unaffected	Heterozygous (A/T)	Heterozygous (C/T)
RML0030	Aunkle of B/father and K/Mother	M	43	Unaffected	Heterozygous (A/T)	Heterozygous (C/T)
RML0031	Grandmother of K/mother & B/father	F	67	Unaffected	Heterozygous (A/T)	Heterozygous (C/T)
RML0032	Wife of RML0019	F	33	Unaffected	Wild type	Wild type
RML0033	Cousin of K & B/ Father	F	1 and a half	Unaffected	Wild type	Wild type
RML0034	Father of K	M	47	Unaffected	Heterozygous (A/T)	Heterozygous (C/T)
RML0035	Grandfather of K/father	F	70	Unaffected	Wild type	Wild type
RML0036	Grandmother of K/father	F	67	Unaffected	Heterozygous (A/T)	Heterozygous (C/T)

Appendix 7.3

Informed Consent Form.

موافقة اشتراك في بحث علمي

فريق البحث: د. زيدون صلاح، مرام عيد.

البحث: دراسة متغيرين جينيين على المستوى الجزيئي لتحديد الطفرة المسببة لمرض تصخر العظم لدى العائلات الفلسطينية.

مكان اجراء البحث: مستشفى المطلع.

المراجع الكريم:

انت مدعو للموافقة على اجراء فحوصات على عيناتك حيث تأتي هذه الفحوصات في اطار دراسة علمية يجريها فريقنا بهدف البحث العلمي، فنأمل من حضرتك الموافقة حيث نتعهد من طرفنا بضمان خصوصية المعلومات الطبية بشكل تام.

سنقوم نحن كفريق من الباحثين باخذ جميع الفحوصات التى تم اجرائها على المصابين لتأكد من التشخيص وايضا سيتم سحب عينات من المشاركين بالبحث لغرض عمل بعض الفحوصات عليها وادراجهم في الدراسة مع المحافظة التامة على الخصوصية وابقاء نتائج الفحوصات واسماء المشاركين طي الكتمان.

بامكانكم طلب اي ايضاحات او معلومات من الباحث الذي سيتواصل معكم وذلك لمعرفة السبب المباشر لطلب الفحوصات والعينات، تجدر الاشارة انه لا يترتب على مشاركتك في هذه الدراسة اي اثار جانبية او تكاليف للفحوصات التي سيتم اجراؤها.

ختاما، ان مشاركتك في البحث تسهم في فهم أفضل لطفرة الجينية المسببة لمرض تصخر العظم في عائلتك والتي قد تفيد مستقبلا في اتخاذ الاجراء المناسب بخصوص كل حالة.

موافقة المشترك

لقد قرأت استمارة القبول هذه وفهمت مضمونها، وبعد الاجابة على كل الاستفسارات التي احتاج اليها. وعليه فإنني حرا مختارا اوافق على الاشتراك في البحث واستخدام العينات والنتائج لاغراض البحث العلمي

اسم المشترك : توقيع المشترك: التاريخ:

Appendix 7.4

The Research Ethical Committee (REC) at Augusta Victoria Hospital (AVH) Approval.

Augusta Victoria Hospital
مستشفى الأوغستا فكتوريا - المطلع

THE LUTHERAN WORLD FEDERATION

لجنة الأخلاق الطبية

Medical Ethics Committee

Ref. No.20/GLD/2024

كتاب طلب عمل دارسة بحثية

أنا الطالب/ ة: Maram Ali Eid من جامعة Al-Quds university،

أتقدّم بالطلب للحصول على معلومات تتعلق بد ارستي البحثية و التي هي بعنوان:

Molecular characterization of two variants in OSTM1 gene in osteopetrosis -affected Palestinian families.

الهدف منها هو:

Our study aims to evaluate the impact of two variants in the OSTM1 gene on the development of osteopetrosis. Although these variants have not been previously identified as pathogenic, their presence in the gene suggests a potential role in the onset of the disease. By doing so, we can raise awareness about the importance of premarital screening for the pathogenic variant of that gene. This knowledge can help identify those at risk and provide preventative therapy, improving patient counseling.

وعليه وبعد الموافقة الرسمية من قبلكم ، أق رّبالالت ازم بمثاق الأخلاق البحثي و المحافظة على حقوق المريض الإنسانية كافة و عدم إلحاق الأذى أو / الضرر بالمريض بطريقة مباشرة أو غير مباشرة، و أتعهد بأن تكون كافة المعلومات التي يتاح لي الوصول إليها خلال فترة جمع المعلومات المتعلقة بالد ارسة المذكورة أعلا ه فقط ، ومن خلال فترة تعاملي مع مرضى مستشفى ال مطّلع و/ أو وثائق لها علاقة بالمرضى و/ أو الملفات الخاصة بالمستشفى و/ أو ممتلكاته ، سأبقي المحافظة عليها بكامل السرية ولن يتم استخدامها بشكل مطلق وقطعي بغير هدف الد ارسة ال محددة أعلاه فقط، ولن أ عطي هذه المعلومات لأي جهة أو/ و شخص كان وتحت أي ظرف كان.

Augusta Victoria Hospital
مستشفى الأوغستا فكتوريا - المطلع

THE LUTHERAN WORLD FEDERATION

لجنة الأخلاق الطبية
Medical Ethics Committee

إن أي معلومة أو وثيقة و/ أو نتيجة مقابلة لمريض و/ أو لأي من ذويه تكون بموافقة لجنة الأخلاق الطبية الخاصة بالمستشفى أولا ا، ثم بموافقة المريض /ة الذي يستطيع أخذ ق ارر وقاد ار على ذلك دون إك اره أو إجبار وبشكل طوعي وإ اردي، وله الحق بالإستسفسار والسؤال عن سبب ومصير المعلومات ، وله الحق بالإنسحاب و/ أو التوقف عن المشا ركة في أي وقت كان، دون إك اره أو إجبار أو أي مساس في حقوقه، وينطبق ذلك على ولي أمر المريض الشرعي و/ أو القانوني في أخذ الق ارر .

توقيع الطالب / ة : Maram Eid

التاريخ : 1/5/2024

مرفق قارر رئيس اللجنة

تحت بموافقة اللجنة على اجراء البحث المذكور أعلاه مع الالتزام باحترام الخصوصية.

Dr. Mamdouh Aker
Head of Medical Ethics Committee
Augusta Victoria Hospital
Tel. 02 - 6279911

- الرجاء إرفاق الوثائق التالية:
  - نموذج موافقة المريض(Informed Consent)
  - نموذج مشروع البحث كامل ا(Proposal of the Study)

Appendix 7.5

WES test results for the three affect patients. The results of the WES analysis revealed that one of the affected patients carried two homozygous variants of uncertain significance in the OSTM1 gene. In contrast, the other two affected patients each had only one variant, which was one of the two identified in the first patient.

Patient 1

OSTM1, p.Val122Asp

The *OSTM1* variant c.365T>A p.(Val122Asp) causes an amino acid change from Valine to Aspartate at position 122. The comparison of *OSTM1* amino acid sequences derived from numerous species indicates that the Val122 is not well-conserved (conserved in 9/16 species). Valine and aspartic acids are dissimilar amino acids. However, the lack of high conservation suggests that the Val122Asp may represent a neutral variant (PMID:23772242), Currently, it is classified as variant of uncertain significance (class 3) according to the recommendations of ACMG.

OSTM1, p.Gly36Gly

The *OSTM1* c.108C>T p.Gly36Gly variant is a silent variant that does not result in an amino acid substitution (GGC and GGT are both codons for glycine). However, the c. 108C > T transition may create a new donor splice site (GT) and result in aberrant mRNA processing.

Patient 2

DETECTED SNV VARIANTS

Gene/ID#	Variant	Zygosity	Disorder	Inheritance	Variant Classification
OSTM1 NM_014028.4	c.365T>A p.Val122Asp	Homozygous	Osteopetrosis, Autosomal Recessive 5	Autosomal Recessive	Uncertain Significance/ Likely Pathogenic

Patient 3

RESULTS:

Single nucleotide variation (SNV) analysis:

Gene	Position	Nucleotide	Amino Acid	GnomAD	dbSNP	Zygosity
OSTM1	6:108395491	c.365T>A	p.Val122Asp	0		Homozygous

Appendix 7.6

Family co-segregation Analysis by Istishari Arab This analysis was conducted for the first patient who was found to be homozygous for the c.108C>T and c.365T>A variants through whole exome sequencing (WES). The analysis indicated that both parents of the affected individual are carriers of both variants, confirming that the patient is homozygous for these two variants.

	Status	Result
– Father	Unaffected	Heterozygous for *OSTM1, p.Val122Asp*
Mother	Unaffected	Heterozygous for *OSTM1, p.Val122Asp*
n	Affected	Homozygous for *OSTM1, p.Val122Asp*
– Father	Unaffected	Heterozygous for *OSTM1, p.Gly36Gly*
Mother	Unaffected	Heterozygous for *OSTM1, p.Gly36Gly*
n	Affected	Homozygous for *OSTM1, p.Gly36Gly*

دراسة متغيرين جينيين في OSTM1 جين على المستوى الجزيئي لتحديد الطفرة المسببة لمرض تصلب العظم لدى العائلات الفلسطينية

إعداد: مرام علي عيد

إشراف: د. زيدون صلاح

الملخص

المقدمة: داء تصلب العظام هو اضطراب وراثي نادر يتميز بزيادة كثافة العظام كما ويسبب هشاشة العظام في الوقت نفسه. تنجم معظم الاصابات عن طفرات تؤثر على العضيات المرتبطة بالعضيات الليزوزومية. يعد جين OSTM1 أحد الجينات المرتبطة بداء تصلب العظم, حدوث طفرات في هذا الجين مرتبطة بشكل وثيق بمرض تصلب العظم الخبيث عند الاطفال الذي يعتبر من اشد انواع هذا المرض خطورة واسوؤها من الناحية التشخصية. في منتصف العام تم إجراء اختبار التسلسل الكامل للإكسوم (WES) على مجموعة من العائلات الفلسطينية المصابة، اظهرت نتيجة الفحص عن وجود متغيرين c.365T>A و c.108C>T في جين OSTM1 لدى المصابين. وجد لاحقا ان هذين المتغيرين لم يتم تصنيفهما من قبل باعتبارهما مسبّبين للمرض. ولذلك، تهدف الدراسة إلى تحديد مدى إسهامهما في الإصابة بمرض التصلب العظمي.

المنهجية: من أجل تقييم القدرة الإمراضية لهذين المتغيرين الجينيين، تم استخراج الحمض النووي والحمض النووي الريبي من كل فرد من أفراد العائلة المشاركة. ومن ثم تم الحصول على الحمض النووي من الدم المحيطي باستخدام MagLEAD 12Gcوهي أداة تستخدم لاستخلاص الحمض النووي التى تعمل بشكل آلي بالكامل، بينما تم عزل الحمض النووي الريبي باستخدام مادة التريزول TRIZOL الجاهزة للاستخدام وفقًا لتعليمات الشركة المصنعة. في بادء الامر تم إجراء تحليل للمتغيراين المعنيين على عينات الحمض النووي المعزولة من المتطوعين المصابين وعائلاتهم الممتدة بواسط Sanger sequencingوذلك باستخدام primers محيطة بمواقع المتغيرات. أما بالنسبة للمتغير c.108 C>T ، الذي يُفترض أنه سيسبب بانشاء RNA معطوب، فقد أُجري تحليل للحمض النووي الريبي الRNA باستخدام Primers تحيط بالإكسونين الأول والثاني لتحديد ما إذا كان ينتج عن هذا المتغير بروتين غير طبيعي نتيجة لتغير النيوكليوتيدي الذي من المتوقع حدوثه في جين OSTM1.

النتائج: من خلال تحليل طريقة وراثة المتغيرين لدى 36 مشاركًا في البحث باستخدام Sanger sequencing تم الحصول على النتائج التالية: أن الأفراد غير المصابين بالمرض كلا المتغيرين تم توريثهما معا اما في حالة Heterozygous او Wild-Type، في حين أن الأفراد المصابين بتصلب العظم حدث تغير نيوكليوتيدي بشكل كامل في كلا المتغيرين (Homozygous).كما وأشار تحليل Electropherograms إلى وجود نمط وراثي متنحٍ كما هو معروف سابقا وان كلا المتغيرين مقترنان وينتقلان معا على نفس الاليل. بالإضافة إلى ذلك، تم إجراء تحليل الحمض النووي الريبي (RNA) للمتغير c.108 C>T في جين OSTM1. وأظهر التحليل أنه خلافًا للاعتقاد السابق، فإن الطفرة لم تنشئ موقعًا جديدا للربط على مستوى الRNA (New Splicing-Site).

الخاتمة: لقد أتاحت هذه الدراسة فرصة للكشف عن المتغير الجيني المسؤول عن المرض في العائلات المشمولة. يمكن أن تساعد هذه المعرفة في تحديد الأشخاص المعرضين للخطر وتوفير العلاج الوقائي، بالإضافة إلى تحسين المشورة للمرضى وزيادة الوعي حول أهمية الفحص قبل الزواج للكشف عن المتغير المسبب للمرض في جين OSTM1. يمكن أن تُسهم الأبحاث المُستمرة في مساعدتنا على فهم الآثار المترتبة على هذه النتائج على الصحة بشكل عام ومساعدة عدد لا يحصى من العائلات على أن تكون أكثر استعداداً للتعامل مع مضاعفات مرض تصلب العظام.